*Q. J. R. Meteorol. Soc.* (1988), **114**, pp. 31–60 551.509.313:551.509.542:551.515.41

# A comparison of explicit and implicit predictions of convective and stratiform precipitating weather systems with a meso-$\beta$-scale numerical model

By DA-LIN ZHANG

*National Center for Atmospheric Research*[1], *Boulder, CO* 80307

EIRH-YU HSIE[2]

*Aeronomy Laboratory, Environmental Research Laboratories/NOAA, Boulder, CO* 80303

and

MITCHELL W. MONCRIEFF

*National Center for Atmospheric Research*[1], *Boulder, CO* 80307

(Received 7 April 1987; revised 21 July 1987)

SUMMARY

The feasibility of the implicit (parametrized) compared to the explicit (grid-resolved) approach for meso-$\beta$-scale models is examined using two different mesoscale precipitating weather systems (MPWSs): a squall line and a mesoscale convective complex (MCC) with an embedded meso-vortex, that were responsible for the 1977 Johnstown, Pennsylvania, flood events. The prognostic explicit scheme contains predictive equations for cloud water and rainwater incorporating liquid water evaporation and hydrostatic water loading, and it is tested with grid sizes of 25 and 12·5 km, respectively. Due to a near-saturated and moist adiabatic initial environment associated with the MPWSs, there is no notable delay in the initiation of the grid-box saturation. It is found that the explicit convective scheme fails to reproduce the convective precipitation related to the squall line and MCC, while it overpredicts the stratiform rainfall associated with the meso-vortex. On the other hand, the implicit convective scheme reproduces the size, orientation and evolution of the squall line, but totally misses the meso-vortex. A semi-implicit control simulation (implicit plus diagnostic explicit) reproduces very well both the squall line and MCC. The results indicate that even with a grid resolution on the order of 10 km, an implicit convective scheme is very important for the numerical prediction of convectively driven precipitating systems.

The roles of different model physics in controlling the frequent model 'blow-ups' are also examined. It is found that if the semi-implicit or the explicit convective scheme is used alone, the model sustains different degrees of overdevelopment of the mesocyclogenesis due to the CISK-like feedback process among latent heat release, larger-scale moisture convergence and the surface pressure fall. Model simulation with the diagnostic explicit scheme is the most affected by this instability, followed by the prognostic explicit scheme. The parametrized convection tends to reduce or eliminate this problem by elevating the heating and moistening maximum and removing moisture that otherwise would be used for explicit condensation. The liquid water evaporation is very effective in an unsaturated environment whereas the hydrostatic water loading has a significant retarding effect under saturated conditions.

Intercomparisons of six experimental simulations in addition to the control run indicate that the combination of the implicit and prognostic explicit schemes (full physics) is superior in reproducing the basic sequence of convective and stratiform rainfall and the extent of the mesocyclogenesis associated with the Johnstown MPWSs. Because of their different roles in handling various types and scales of precipitation, the full physics approach appears to allow a broader scale interaction between the parametrized convection and mesoscale environment and to have the greatest potential success in predicting MPWSs that occur under various environmental conditions.

## 1. INTRODUCTION

The treatment of convective processes in large-scale and mesoscale models as the grid resolution continues to improve is a fundamental problem in numerical weather prediction (see Frank 1983). One of the issues to be quantified is the extent to which convection can be explicitly resolved (the explicit approach) in high resolution models or whether there is a basic necessity to continue to parametrize convective transports (the implicit approach). It is well accepted that individual convective clouds are explicitly

[1] The National Center for Atmospheric Research is funded by the National Science Foundation
[2] Also affiliated with the Cooperative Institute for Research in Environmental Sciences

resolvable by meso-$\gamma$-scale (as defined by Orlanski (1975)) cloud models (e.g. Moncrieff and Miller 1976; Cotton and Tripoli 1978; Klemp and Wilhelmson 1978; Clark 1979), whereas for numerical models with grid resolution on the order of hundreds of kilometres, deep convective elements are considered as subgrid processes and their collective effects have to be parametrized by resolvable-scale variables (e.g. Anthes and Warner 1978; Phillips 1978). However, for a grid resolution between these two scales, i.e. used to resolve meso-$\alpha$ and $\beta$-scale features, the choice between explicit and implicit representations of deep convection is not so obvious, since a well-developed convective cloud system can have a mesoscale dimension whereas its initial convective development and individual cells are not resolvable. For historical reasons, most meso-$\alpha$ and larger-scale models contain an implicit convection scheme and a diagnostic formulation to compute resolvable-scale condensation (the semi-implicit approach).

Recently, there have been contradictory reports in the literature with regard to the use of explicit versus implicit methods for meso-$\alpha$-scale models. For instance, both Ross and Orlanski (1982) and Hsie *et al.* (1984) explicitly simulated frontogenesis processes using, respectively, a grid element of 61·5 km with real data and 40 km with an idealized initial condition. Their simulations favour the use of the explicit approach, although the detailed comparisons were not available. The success with the explicit approach by Ross and Orlanski (1982) is due to the fact that they utilized an eddy viscosity which becomes very large under convectively unstable conditions. By contrast, with a similar grid resolution for the simulation of an observed mesoscale convective complex (MCC), Molinari and Dudek (1986) found that an explicit simulation produced localized excessive rainfall due to a runaway type of positive feedback among latent heat release, larger-scale moisture convergence, and surface pressure fall. Kalb (1987) also reported the excessive rainfall 'blow-ups' associated with a frontal precipitation system with an explicit representation of moist physics. Similar features can often be observed in daily operational forecasts produced with semi-implicit approaches such as the limited-area fine-mesh model (LFM), the regional analysis and forecast system (RAFS) and the European Centre for Medium-range Weather Forecasts (ECMWF). Such runaway feedback instability is referred to here as an *unrealistic* development of the conditional instability of the second kind (or *CISK-like* instability) that appears to result from the neglect of certain resolvable and subgrid-scale retarding factors. A thorough discussion on this subject will be given in section 5 of this paper. Another common problem associated with meso-$\alpha$ and larger scale explicit models is an unrealistic delay in resolvable-scale condensation due to the long duration which is required for the start of the grid-box saturation by the resolvable-scale circulation. This has also been indicated by Molinari and Dudek (1986) and Kalb (1987). The findings of both tend to suggest that an explicit approach is not suitable for meso-$\alpha$-scale numerical models.

On the meso-$\beta$ scale, two different types of numerical models are currently used to investigate mesoscale precipitating weather systems (MPWSs) with both explicit and implicit methods. The first type is from the *upper* part of the spatial scale progressing downwards using hydrostatic models. In this group, Fritsch and Chappell (1980) and Frank and Cohen (1985) developed cumulus parametrization schemes suitable for grid resolution down to 20–30 km. Zhang and Fritsch (1986a) showed that a semi-implicit simulation with a grid spacing of 25 km produced excellent structure and evolution of convective and stratiform precipitating weather systems that were associated with the 1977 Johnstown, Pennsylvania (U.S.A.), flash flood. (The term stratiform is used rather loosely here, since Leary and Rappaport (1987) have shown that, at least in some instances, the so-called stratiform regions are actually marginally convective. A more appropriate term, from the numerical modelling standpoint, is 'resolvable-scale' precipi-

tation.) At the same time, Zhang and Fritsch (1987a, b) noted that although the saturation delay, which is often a problem for meso-$\alpha$ and larger-scale models, is not an issue on the meso-$\beta$ scale, the treatment of the CISK-like instability becomes a more challenging factor for the meso-$\beta$-scale numerical studies because of the increase in resolvable-scale convergence/divergence. In contrast, with a similar grid resolution, Rosenthal (1979) noticed that the simulated hurricane development is highly sensitive to the details of convective parametrization. Rosenthal (1978) found that an explicit representation of moist physics had the advantage of allowing a broad spectrum of interaction between resolved mesoscale convection and the larger-scale environment. Similarly, Brown (1979) successfully simulated mesoscale unsaturated downdraughts associated with rainfall evaporation using an explicit approach. With a much smaller grid spacing ($\Delta x = 10\,\text{km}$), Nickerson *et al.* (1986) showed that an explicit convective scheme with detailed parametrized microphysics was capable of simulating orographically forced clouds, rainfall and airflow. All these meso-$\beta$-scale studies with explicit methods are limited to the use of idealized initial conditions.

The second type of model used for meso-$\beta$-scale numerical studies is from the *lower* end of the spatial scale progressing upwards using nonhydrostatic models. For most of those studies, the numerical models contain sophisticated microphysics with explicitly resolved convective systems (e.g. Yamasaki 1977; Lord *et al.* 1984; Rotunno and Emanuel 1987). The grid resolution they used ranges from a few hundred metres to tens of kilometres. Nevertheless, it is very interesting to note a recent report by Pointin (1985) who developed a time-dependent parametrized convective scheme coupled with a non-hydrostatic model with 5 km grid spacing. He believed that such a grid size is still too large to resolve explicitly the internal structure of convective elements, such as updraughts, downdraughts and precipitation fallout. Thus, on the meso-$\beta$ scale, there is little confidence in establishing whether or not an explicit approach should perform better than an implicit method, or vice versa, particularly with hydrostatic models.

According to the definition, an explicit approach requires grid-scale saturation prior to the occurrence of rainfall, and assumes that convective effects due to subgrid eddy fluxes (i.e. the term $(L/c_p)\overline{C^*} - \partial\overline{\omega' T'}/\partial p$ in the thermodynamic equation) can be neglected when compared with the resolvable-scale vertical transport. Hence, after considering the above 'contradictory' reports, it is hypothesized that success with an implicit versus an explicit approach may depend upon *the particular precipitating mode*: *convective* versus *stratiform*, and *the larger-scale forcing type*: *quasi-stationary* versus *propagating* and *weak* versus *strong baroclinicity*. Of course, it is important that the grid resolution used be compatible with the scale and type of the weather phenomenon being studied. A test of the above hypothesis for meso-$\beta$-scale models is one of the themes of the present study, another theme is to examine the roles of implicit and explicit convective schemes in the more realistic handling of the CISK-like instability in meso-$\beta$-scale models.

In order to make this study as relevant as possible, a real data case of the MPWSs that were responsible for the Johnstown flood events (hereafter referred to as the Johnstown MPWSs) is selected. This particular case is chosen because: (1) there were two types of MPWSs involved: first, a convective squall line; second, a stratiform MCC; (2) the Johnstown MPWSs developed in a summertime weak-gradient synoptic situation instead of in a strongly forced environment (i.e. strong positive vorticity advection, thermal advection and/or frontal lifting). The MPWSs were therefore basically driven by *the sources and sinks of the convective heating rather than by the larger-scale system.* Evidently, such a situation provides a great opportunity for a test of different explicit and implicit convective schemes; (3) the MPWSs have been well documented by Hoxit *et al.* (1978) and Bosart and Sanders (1981), and also well simulated by Zhang and Fritsch

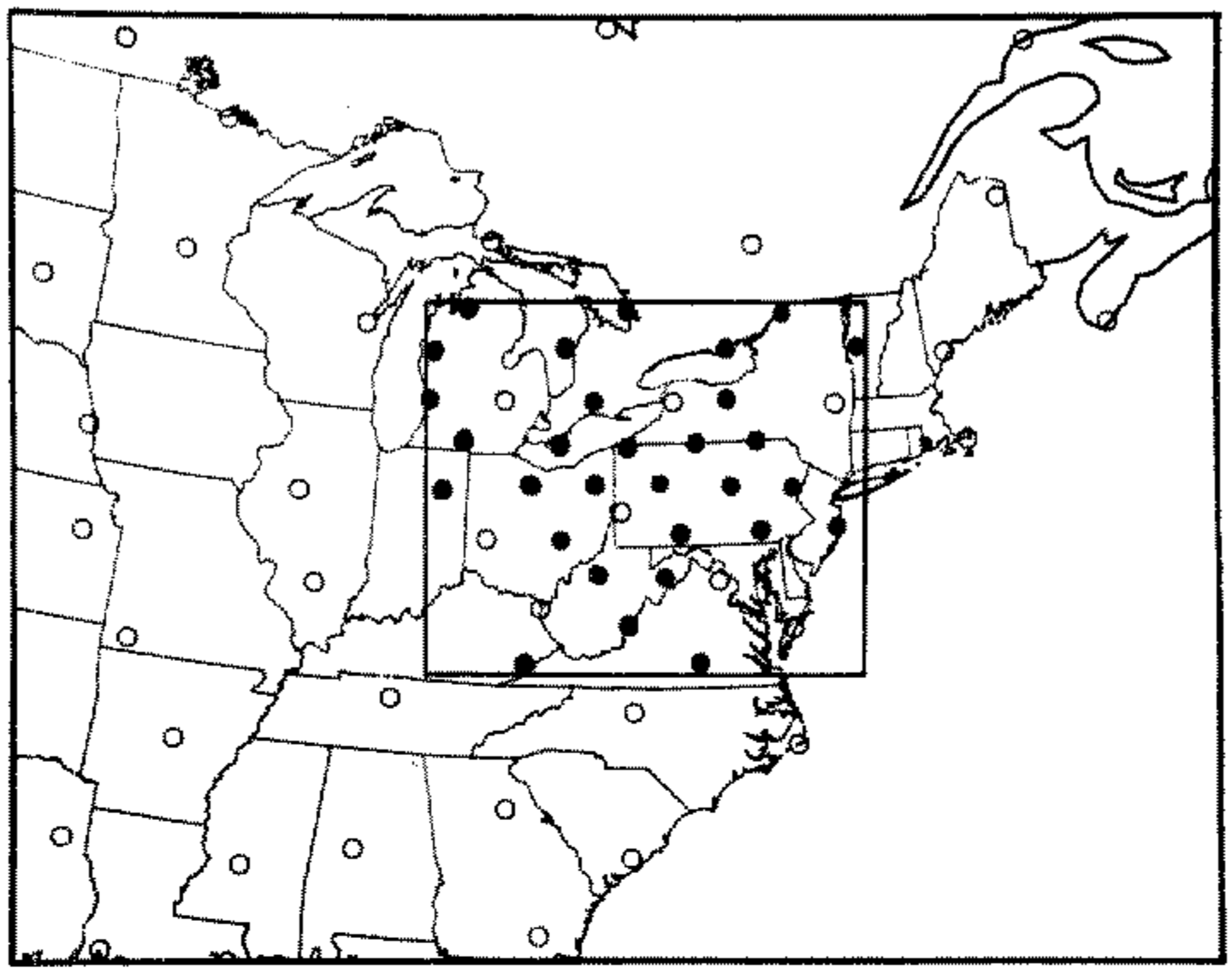

Figure 1. Nested-grid domain with the distribution of regular rawinsonde stations (open circles) and the Bosart sounding locations (solid circles). The interior thick solid lines denote the mesh interface.

(1986a) so that strict and careful comparisons can facilitate the understanding of the simulation of the MPWSs; (4) the subjectively analysed soundings by L. Bosart (personal communication, 1982) fill gaps in the low density of the standard observations and make the present meso-$\beta$-scale comparative study possible (see Fig. 1 for the density of soundings used for this study).

Section 2 presents the primary physics in the model and describes the control simulation; section 3 provides the experimental design for this study; section 4 shows the comparison of the implicit versus explicit simulations; and section 5 discusses the feasibility of the explicit approach in the mesoscale models and the possible prevention of CISK-like instability. Concluding remarks are given in the last section.

## 2. Model description and control simulation

In order to obtain a better physical representation for simulating different mesoscale convective systems, the Pennsylvania State University/NCAR three-dimensional hydrostatic mesoscale model originally developed by Anthes and Warner (1978) has been modified with the following numerical and physical aspects now incorporated:

(i) an explicit calculation of both cloud water and rainwater as time-dependent variables (see Hsie *et al.* 1984);
(ii) a modified version of the Fritsch–Chappell (1980) convective parametrization (see Zhang and Fritsch 1986a) for the fine-mesh and an R. A. Anthes–H. L. Kuo type of convective scheme (Anthes and Keyser 1979) for the coarse-mesh portions of the nested-grid model;
(iii) a two-way interactive nested-grid procedure (Zhang *et al.* 1986);
(iv) a modified version of the Blackadar 'large-eddy exchange' planetary boundary layer (PBL) parametrization (Zhang and Anthes 1982; Zhang and Fritsch 1986a); and
(v) 'sponge' lateral boundary conditions (Perkey and Kreitzberg 1976) for the outermost coarse-mesh boundary.

The nested-grid ratio is 1 to 3 with a fine-mesh length of 25 km and a coarse-mesh

length of 75 km. The $(x, y, \sigma)$ dimensions of the coarse and fine meshes are $39\times31\times19$ and $43\times37\times19$, respectively. The vertical coordinate $\sigma$ is defined as

$$\sigma = (p - p_t)/p^* \tag{1}$$

where

$$p^* = p_s - p_t \tag{2}$$

and $p_t$ and $p_s$ are the pressures at the top of the model and at the surface, respectively. The value of $p_t$ is 80 mb in this case. Figure 1 shows the model domain of both fine and coarse meshes for this study. Since the results from the fine-mesh domain are of essential interest, the following discussions will be confined only to the fine-mesh results. The complete governing system includes seven prognostic equations for momentum $(u, v)$, temperature $(T)$, total mass $(p^*)$, water vapour $(q_v)$, cloud water $(q_c)$, and rainwater $(q_r)$, and three diagnostic equations for geopotential height, $\phi$, vertical velocities in both $p$ coordinate, $\omega$, and $\sigma$ coordinate, $\dot{\sigma}$. They are given as follows:

$$\frac{\partial p^* u}{\partial t} = -m^2\left[\frac{\partial(p^* u\,u/m)}{\partial x} + \frac{\partial(p^* v\,u/m)}{\partial y}\right] - \frac{\partial p^* u\dot{\sigma}}{\partial \sigma} + fp^* v - mp^*\left(\frac{RT_v}{p^* + p_t/\sigma}\frac{\partial p^*}{\partial x} + \frac{\partial \phi}{\partial x}\right) + (F_{CON} + F_{PBL} + F_{HD} + F_{VD})p^* u \tag{3}$$

$$\frac{\partial p^* v}{\partial t} = -m^2\left[\frac{\partial(p^* u\,v/m)}{\partial x} + \frac{\partial(p^* v\,v/m)}{\partial y}\right] - \frac{\partial p^* v\dot{\sigma}}{\partial \sigma} - fp^* u - mp^*\left(\frac{RT_v}{p^* + p_t/\sigma}\frac{\partial p^*}{\partial y} + \frac{\partial \phi}{\partial y}\right) + (F_{CON} + F_{PBL} + F_{HD} + F_{VD})p^* v \tag{4}$$

$$\frac{\partial p^* T}{\partial t} = -m^2\left[\frac{\partial(up^* T/m)}{\partial x} + \frac{\partial(vp^* T/m)}{\partial y}\right] - \frac{\partial p^* T\dot{\sigma}}{\partial \sigma} + \frac{RT_v\omega}{c_{pm}(\sigma + p_t/p^*)} + \frac{L_v p^*(P_{con} - P_{re})}{c_{pm}} + (F_{CON} + F_{PBL} + F_{HD} + F_{VD})p^* T \tag{5}$$

$$\frac{\partial p^* q_v}{\partial t} = -m^2\left[\frac{\partial(up^* q_v/m)}{\partial x} + \frac{\partial(vp^* q_v/m)}{\partial y}\right] - \frac{\partial p^* q_v\dot{\sigma}}{\partial \sigma} - p^*(P_{con} - P_{re}) + (F_{CON} + F_{PBL} + F_{HD} + F_{VD})p^* q_v \tag{6}$$

$$\frac{\partial p^* q_c}{\partial t} = -m^2\left[\frac{\partial(up^* q_c/m)}{\partial x} + \frac{\partial(vp^* q_c/m)}{\partial y}\right] - \frac{\partial p^* q_c\dot{\sigma}}{\partial \sigma} + p^*(P_{con} - P_{ra} - P_{rc}) + (F_{PBL} + F_{HD} + F_{VD})p^* q_c \tag{7}$$

$$\frac{\partial p^* q_r}{\partial t} = -m^2\left[\frac{\partial(up^* q_r/m)}{\partial x} + \frac{\partial(vp^* q_r/m)}{\partial y}\right] - \frac{\partial p^* q_r\dot{\sigma}}{\partial \sigma} + p^*(P_{ra} + P_{rc} - P_{re}) - g\frac{\partial(\rho q_r v_t)}{\partial \sigma} + F_{HD}\,p^* q_r \tag{8}$$

$$\frac{\partial p^*}{\partial t} = -m^2\left[\frac{\partial(p^* u/m)}{\partial x} + \frac{\partial(p^* v/m)}{\partial y}\right] - \frac{\partial p^*\dot{\sigma}}{\partial \sigma} \tag{9}$$

$$\dot{\sigma} = \frac{1}{p^*}\int_1^\sigma \left\{\frac{\partial p^*}{\partial t} + m^2\left[\frac{\partial(p^* u/m)}{\partial x} + \frac{\partial(p^* v/m)}{\partial y}\right]\right\} d\sigma' \tag{10}$$

$$\omega = p^*\dot{\sigma} + \sigma\left[\frac{\partial p^*}{\partial t} + m\left(u\frac{\partial p^*}{\partial x} + v\frac{\partial p^*}{\partial y}\right)\right] \tag{11}$$

$$\frac{\partial \phi}{\partial \ln(\sigma + p_t/p^*)} = -RT_v\left[1 + \frac{q_c + q_r}{1 + q_v}\right]^{-1} \tag{12}$$

where

$$T_v \equiv T(1 + 0{\cdot}608q_v) \tag{13}$$

is the virtual temperature, and

$$c_{pm} = c_p(1 + 0{\cdot}81q_v) \tag{14}$$

is the specific heat at constant pressure for moist air, $F_{CON}$, $F_{PBL}$, $F_{HD}$, and $F_{VD}$ are the tendency operators for parametrized moist convection, the PBL effect, horizontal diffusion, and vertical diffusion, respectively, $P_{ra}$ is the accretion rate of cloud droplets by raindrops, $P_{rc}$ the autoconversion rate of cloud droplets to raindrops, $P_{re}$ the evaporation rate of raindrops, $P_{con}$ the condensation rate of water vapour or the evaporation rate of cloud droplets, and $v_t$ the mass-weighted mean terminal velocity of raindrops, and all other variables assume their meteorological meaning. The microphysical treatments in Eqs. (6)–(8) follow Kessler (1969), Liu and Orville (1969), Orville and Kopp (1977) and Asai (1965). Hsie *et al.* (1984) provide a detailed description of the explicit formulations. Note that the only microphysics omitted in this model are phase changes associated with frozen particles. Although the importance of ice phase microphysics in hydrostatic models remains to be rigorously tested, Lord *et al.* (1984) showed in a nonhydrostatic model that the ice microphysics influences the distribution of condensate in the cloud anvil associated with a model hurricane. The virtual temperature (Eq. (13)) and hydrostatic water loading (Eq. (12)) effects have been included in the governing equations. The virtual temperature effect is particularly important for simulating MPWSs since the usual higher moisture content in the lower levels will increase parcel buoyancy while low-level drying and upper-level moistening by moist convection tend to produce the virtual effect of low-level cooling and upper-level warming. Another significant effect of using virtual temperature instead of temperature arises because it impacts substantially upon the calculation of the geopotential height. Zhang and Fritsch (1987b) have quantitatively evaluated the effects of virtual temperature on the simulated MPWSs. The importance of the water loading is just to compensate for the virtual temperature effect and this will be quantitatively examined in the following two sections. For a more detailed description of the different model aspects, the reader is referred to Anthes and Warner (1978), Hsie *et al.* (1984) and Zhang and Fritsch (1986a).

For this study, when an implicit approach is invoked, convective parametrization schemes are adopted while resolvable-scale phase changes are neglected. For a semi-implicit approach, an implicit convective scheme is included and the resolvable-scale supersaturation and associated heating are computed according to a standard formulation (see Haltiner and Williams 1980, p. 318):

$$P_{con} = \begin{cases} \dfrac{(q_v - q_{vs})/\Delta t}{1 + L_v^2 q_{vs}/c_{pm}R_v T^2} & q_v > q_{vs} \\ 0 & q_v \leqslant q_{vs}. \end{cases} \tag{15}$$

Otherwise, the tendency operator $F_{CON}$ from the governing system (3)–(12) is ignored in an explicit simulation. To clarify the nomenclature, the addition of Eqs. (7) and (8) into the governing system is referred to as the prognostic explicit scheme whereas the use of Eq. (15) for the resolvable-scale phase changes is termed the diagnostic 'explicit' scheme.

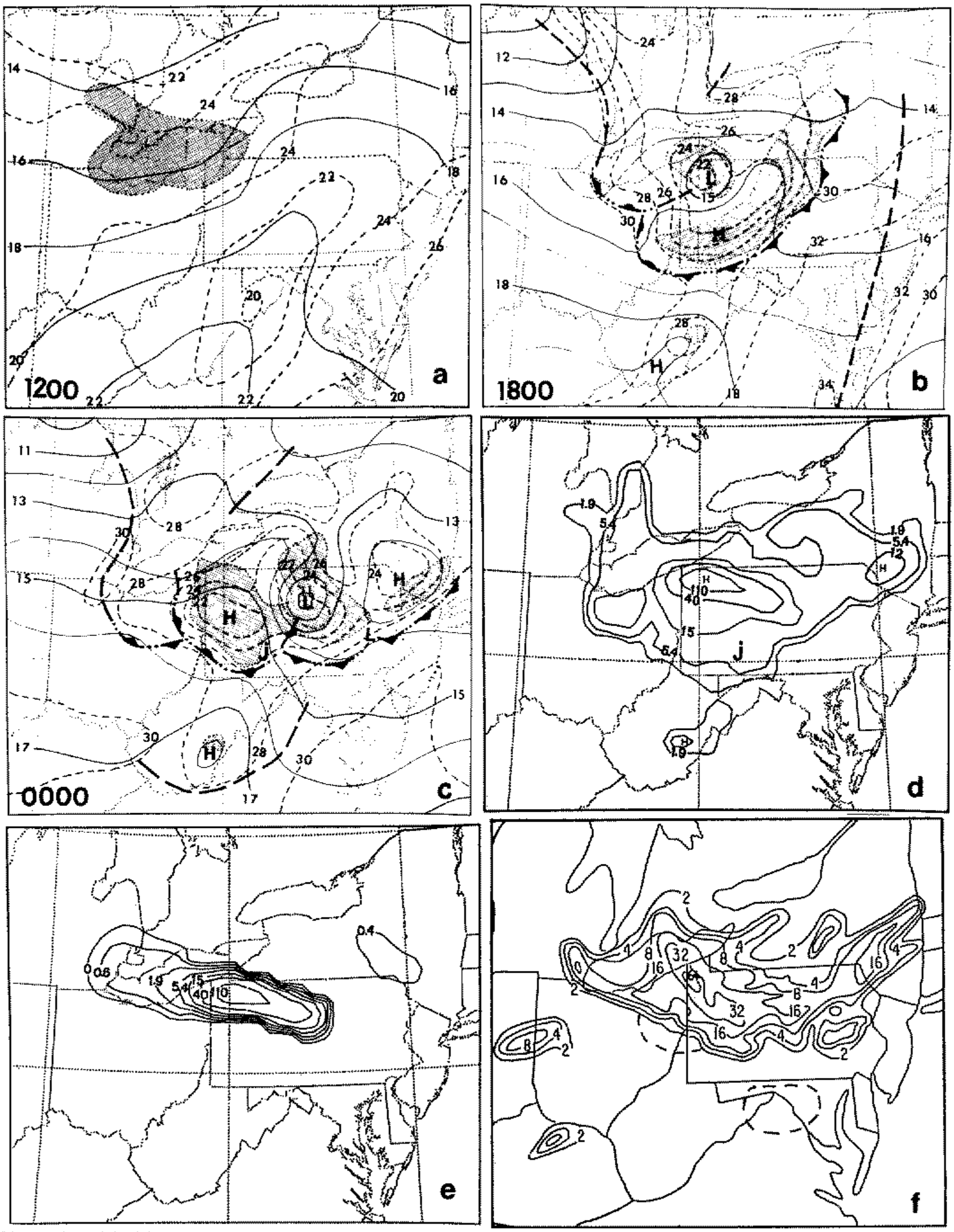


Figure 2. (a)–(c) Analyses of sea level pressure (solid lines, mb) and surface temperature (dashed lines, °C) from exp. CTS (semi-implicit control simulation) for the times indicated. Shading denotes the area of active convection produced by the implicit scheme. Heavy dashed lines indicate troughs; frontal symbols alternated with double dots denote cool outflow boundaries. (d) Predicted 12 h accumulated total rainfall (mm) and (e) resolvable-scale rainfall (mm) for the period 12 GMT 19 to 00 GMT 20 July 1977. (f) As in (d) and (e) but as observed (adapted from Bosart and Sanders (1981)).

As shown in Zhang and Fritsch (1986a), the semi-implicit control simulation (exp. CTS) reproduced very well the size, propagation and orientation of the squall line and the MCC that were associated with the Johnstown flood events. In particular, the simulated evolution of diurnal variations in the PBL, convectively generated outflow

boundaries, low-level jets, surface pressure perturbations (e.g. meso-$\beta$-scale lows, highs, ridges and troughs), a mid-level meso-$\alpha$-scale short wave and the 12 h predicted rainfall distribution and magnitude compare favourably with observational analyses by Hoxit *et al.* (1978) and Bosart and Sanders (1981). Figure 2 shows a portion of the surface features from the semi-implicit control simulation for the purpose of comparison with the experimental simulations. The area of deep convection initially over Lake Erie (Fig. 2(a)) intensifies as it propagates east-south-eastward, and by 18 GMT it has split into two precipitating weather systems (Fig. 2(b)), namely, a squall line and an area of convection that later developed into the MCC responsible for the Johnstown flood (hereafter termed pre-MCC). A distinct mesolow and a corresponding mid-level meso-vortex develop in the same region as the pre-MCC, and they propagate eastward. At 00 GMT (Fig. 2(c)), only the north-eastern portion of the squall line remained active with a trailing meso-high. The simulated 12 h accumulated rainfall is compared with that observed in Figs. 2(d) and (f). The basic patterns are very similar, although the predicted amounts over north-western Pennsylvania are too large compared with the Bosart and Sanders analysis, but very comparable to the Hoxit *et al.* analysis (see Fig. 21(a) in Zhang and Fritsch (1986a)), considering that virtually all the precipitation over this region fell within this 12 h period. Zhang and Fritsch (1987a, b) have established that the positive feedback among the low-level moisture convergence, latent heat release and surface pressure fall is responsible for the natural development of the mesolow/meso-vortex through resolvable-scale condensation. This mechanism appears to result from the near saturated and moist adiabatic stratification over Lake Erie in combination with the centralized upward lifting from the meso-$\alpha$-scale short wave at the model initial time (see Zhang and Fritsch 1986b). However, the grid-point precipitation maximum, mostly associated with resolvable-scale condensation ($\approx$165 mm, see Table 1) and the associated mesolow, are somewhat overgenerated. This is to some degree due to the relatively poor control of the CISK-like instability, as discussed in Zhang and Fritsch (1987a). The orientation of the maximum rainfall over north-western Pennsylvania corresponds to the path of the mesolow/meso-vortex, as indicated by the distribution of 12 h accumulated resolvable-scale rainfall (see Fig. 2(e)). The transverse dimension of the resolvable-scale rainfall distribution roughly reflects the size of the mesolow/meso-vortex. As shown in Table 1, the resolvable-scale condensation made a significant contribution to the total rainfall ($\approx$44%).

## 3. Experimental design

In order to accomplish the objectives of this study, six simulations are conducted. Each has conditions identical to the semi-implicit control simulation except for the treatment of the moist physics. These numerical experiments are designed as follows:

TABLE 1. Predicted 12 h accumulated total rainfall volume of implicit ($R_{Imp}$), explicit ($R_{Exp}$) schemes and point maximum ($R_H$); minimum sea-level pressure ($p_L$) of the mesolow; and point maximum vertical motion ($-\omega_H$) for individual experimental simulations

| Code | Description of simulations | $R_{Imp}$ ($10^{12}$kg) | $R_{Exp}$ ($10^{12}$kg) | $R_H$ (mm) | $p_L$ (mb) | $-\omega_H$ ($\mu$b s$^{-1}$) |
|---|---|---|---|---|---|---|
| CTS | Semi-implicit control | 2·24 | 1·77 | 165 | 1011 | 255 |
| a: DES | Diagnostic explicit | | 3·44 | 315 | 1004 | 485 |
| b: PES | Prognostic explicit | | 2·63 | 187 | 1009 | 324 |
| c: NEV | No evaporation | | 3·03 | 197 | 1007 | 362 |
| d: NWL | No water loading | | 3·18 | 243 | 1007 | 422 |
| e: DHR | Double horizontal resolution | | 2·30 | 255 | 1010 | 550 |
| f: FPS | Full physics | 2·76 | 1·41 | 117 | 1011 | 215 |

(i) *Diagnostic explicit simulation* (*exp.* DES). Due to its attractive simplicity, numerous studies have employed this approach to infer the effect of resolvable-scale condensation on the simulated MPWSs (e.g. Anthes *et al.* 1983; Koch *et al.* 1985; Molinari and Dudek 1986). This method is analogous to the standard technique used in large-scale models to remove the resolvable-scale supersaturation, and it is often referred to as large-scale condensation, stable precipitation or non-convective precipitation. However, because of its unrealistic representation of resolvable-scale physical processes (i.e. instantaneous removal of condensate in a vertical column and the lack of evaporation, melting and water loading), and because of the absence of mechanisms to release the gravitational instability other than through the resolvable-scale penetrative circulation, mesoscale models using this formulation frequently suffer the most from the overdevelopment of cyclogenesis due to the uncontrolled CISK-like instability. Thus, the purpose of this experiment is to show the extent to which the unrealistic CISK-like instability develops in the present meso-$\beta$-scale simulation, and to provide a basis for comparison with other simulations in which the resolvable-scale physics is treated differently.

(ii) *Prognostic explicit simulation* (*exp.* PES). In contrast to exp. DES, liquid water evaporation and water loading are included. Their specific effects on the simulated Johnstown MPWSs will be examined in the experiments next to be described. Here, as the cloud water and rainwater become time-dependently coupled with the resolvable-scale circulations, the horizontal and vertical distribution of resolvable-scale heating and height gradient can be significantly affected since liquid water can be horizontally and vertically advected by the flow, producing a drag on the vertical motion and evaporation on entering an unsaturated environment. This effect can be instrumental in altering the mesoscale structure since many studies have indicated the model's sensitivity to the magnitude and distribution of condensational heating (e.g. Tracton 1973; Koss 1976; Anthes and Keyser 1979). Hence, this simulation is designed not only to investigate the feasibility of an explicit approach for meso-$\beta$-scale models, but also to show the significance of coupling resolvable-scale condensates with model dynamics.

(iii) *Prognostic explicit simulation without evaporation* (*exp.* NEV). The importance of rainfall evaporation in inducing mesoscale downdraughts has been well documented by Zipser (1977), Brown (1979) and Leary and Houze (1979). In a meso-$\alpha$-scale simulation, Molinari and Dudek (1986) have found that both rainfall evaporation and water loading played an important role in retarding the development of CISK-like instability. It is therefore desirable to test this aspect in the present meso-$\beta$-scale model.

(iv) *Prognostic explicit simulation without water loading* (*exp.* NWL). In nonhydrostatic models, the water loading directly suppresses the development of cloud updraughts through the drag effect (Orville *et al.* 1975; Orville and Chen 1982). However, in hydrostatic models, as shown in Eq. (12), water loading compensates for the virtual temperature effect and condensational warming in the calculation of the geopotential height, and the vertical motion is indirectly retarded. In particular, Zhang and Fritsch (1987b) showed that the virtual temperature effect is so crucial that, in its absence, the model failed to reproduce the MCC and mesolow/meso-vortex in the Johnstown flood. Hence, the purpose of this experiment is similar to exp. NEV, as well as to show how the simulated MCC and mesolow/meso-vortex are affected by water loading, since these types of weather systems are often found to be associated with mesoscale heavy stratiform rainfall (see Houze 1977; Maddox 1983; Rockwood *et al.* 1984).

(v) *Prognostic explicit simulation with double horizontal resolution* (*exp.* DHR). The coarse and fine meshes have grid spacings of 37·5 and 12·5 km, and domain $(x, y, \sigma)$

dimensions of 77×61×19 and 85×73×19, respectively. The grid resolution of 12·5 km is as high as can be used in conjunction with the hydrostatic assumption, according to theoretical studies by Orlanski (1981) and Martin and Pielke (1983). Meanwhile, the initial dataset including the Bosart supplementary soundings has a very high resolution and has been well analysed by an experienced synoptician. Thus, the results from this simulation can provide additional information on the performance of explicit versus implicit approaches to the simulation of convective and stratiform precipitating weather systems with a meso-$\beta$-scale model.

(vi) *Full physics simulation* (*exp.* FPS). In this run, the prognostic explicit and implicit operators are all turned on for both meshes (the Anthes–Kuo scheme for the coarse mesh and Fritsch–Chappell scheme for the fine mesh). Such an approach does not account twice for either resolvable-scale or the convective heating and moistening, since the convective eddy fluxes ignored by an explicit approach are included in an implicit convective scheme. (Actually, the concept is similar to the conventional semi-implicit approach.) This implies that an implicit convective scheme provides the effect of sub-grid-scale precipitating convective clouds that form in a conditionally unstable environment without requiring resolvable-scale saturation, while an explicit convective scheme contains the effect of resolvable-scale condensation/evaporation that occur in a saturated atmosphere. Although the cloud water and rainwater are not explicitly present in either the Fritsch–Chappell or Anthes–Kuo parametrization schemes, the present approach will not produce any notable discontinuity in the resolvable-scale dynamics and thermodynamics when the model rainfall switches from convective to stratiform mode. Even in the limit as the stability approaches neutral and saturated conditions, both parametrized and grid-resolved rainfall are expected to be present in the model, but the sensible heat and moisture fluxes tend to diminish. Then, the resolvable-scale diabatic processes gradually take over, thus providing a smooth transition. However, the incorporation of cloud water and rainwater may affect the profiles of parametrized heating and moistening. A similar approach has been successfully applied by Chang *et al.* (1981) and Perkey and Maddox (1985) to the simulation of different MPWSs but with much larger grid sizes. The purpose of conducting this experiment is to examine individual roles of the explicit and implicit convective schemes in reproducing the different weather components of the Johnstown MPWSs and to determine their combined effects on the controlling of the CISK-like instability.

It is considered that these six experiments plus the semi-implicit control simulation permit the evaluation of the performance of explicit versus implicit simulations for the meso-$\beta$-scale precipitating weather systems, and on the improved control of the CISK-like instability in a high resolution hydrostatic mesoscale model.

## 4. Experimental simulations

Generally, the feasibility of the explicit versus implicit approaches for the Johnstown MPWSs and the behaviour of the CISK-like instability can be evaluated from such diagnostic parameters as rainfall, vertical motion and sea level pressure. In addition, for each simulation, Table 1 lists the minimum central pressure of the major mesolow, the 12 h domain-accumulated rainfall volume and the point-accumulated maximum rainfall amount, and the maximum upward motion ($-\omega$) at middle levels. Figures 3 and 4 show, respectively, the hourly rainfall rate, and the maximum area-averaged (2500 km$^2$, i.e. 25-point average for exp. DHR and 9-point average for all others) vertical motion profiles during the 12 h integration period. The individual point vertical motion profiles are not

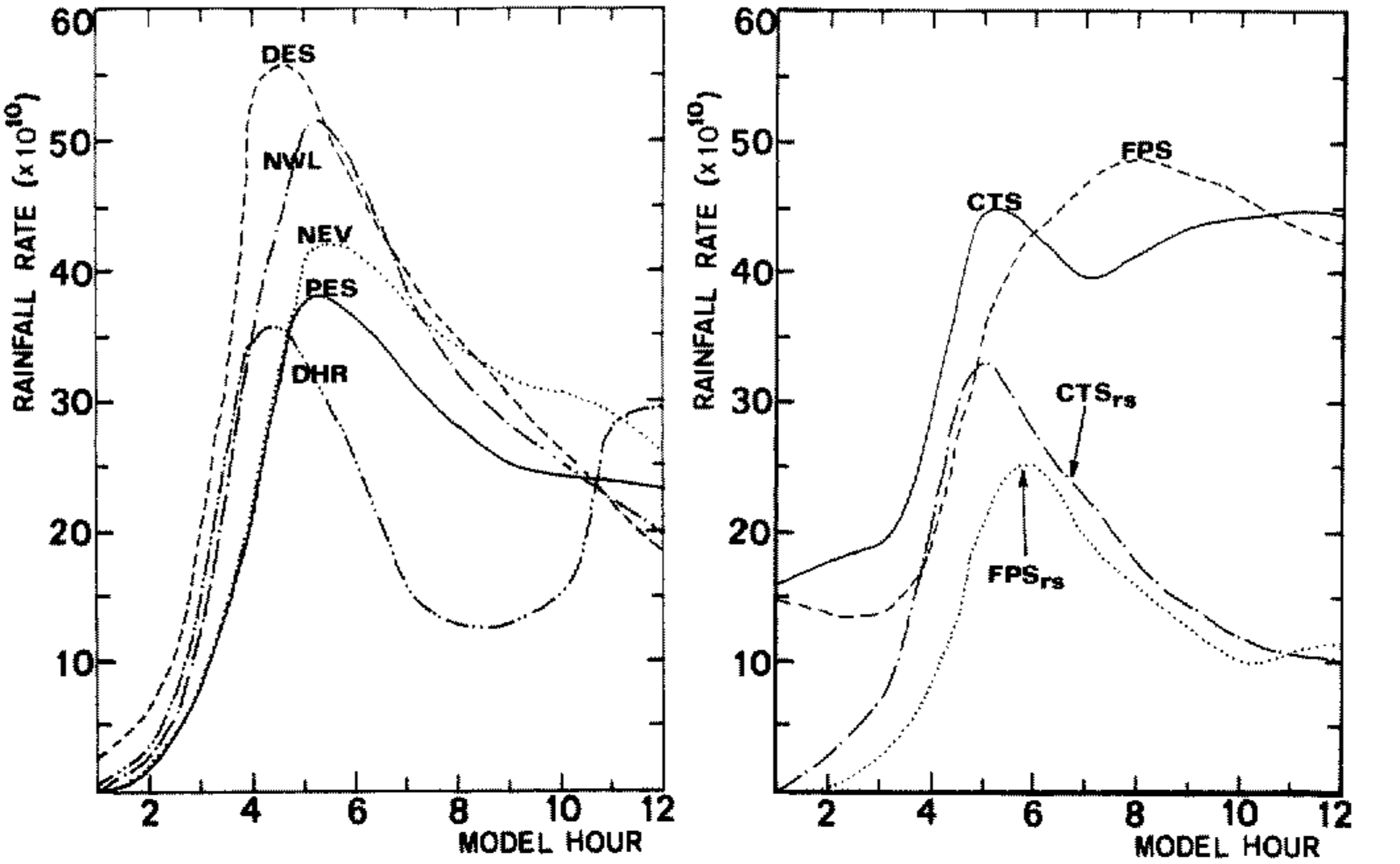


Figure 3. The predicted hourly domain total rainfall rate ($kg\,h^{-1}$) for individual experimental simulations. Subscripts 'rs' denote the resolvable-scale rainfall rate.

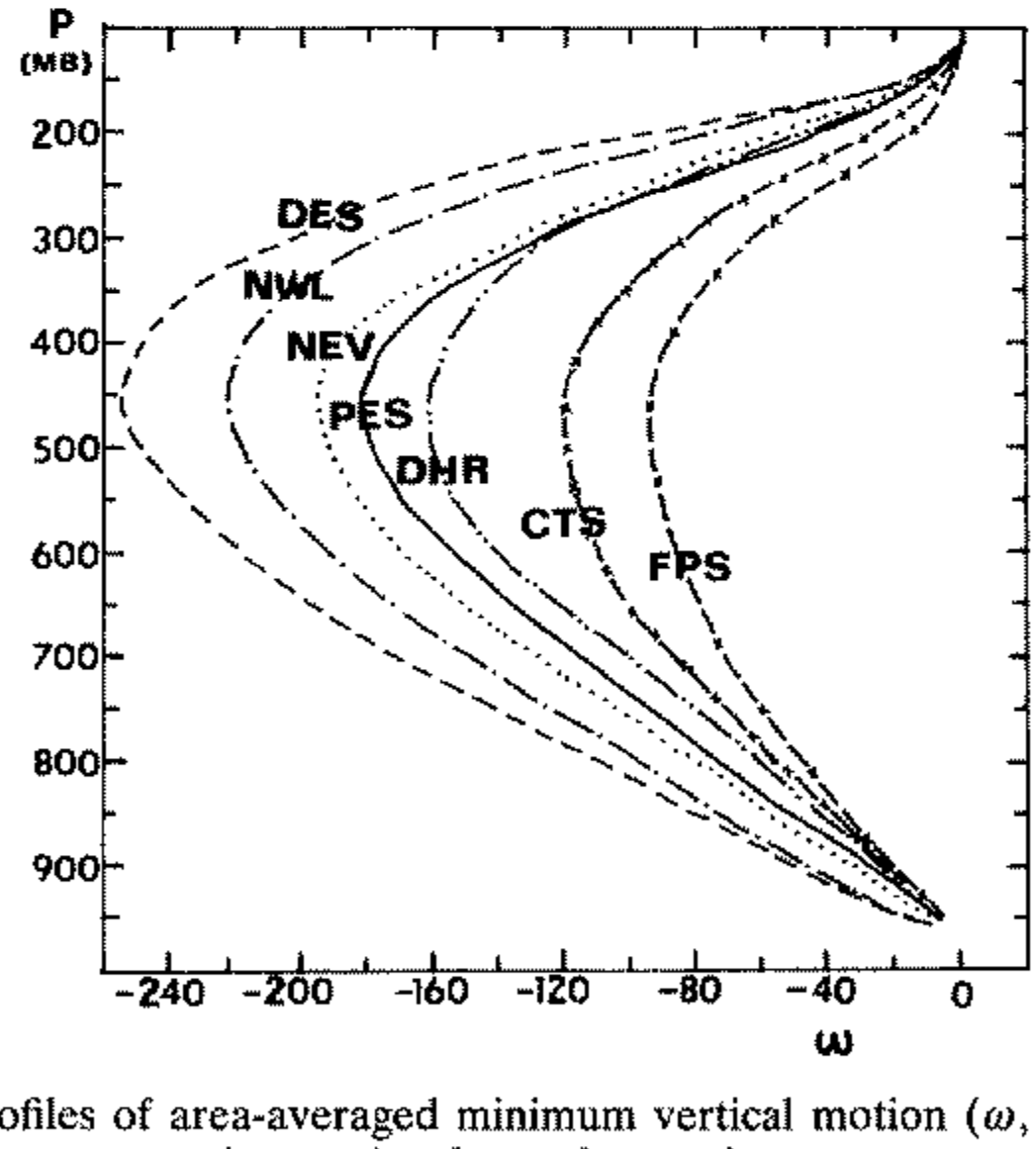


Figure 4. The vertical profiles of area-averaged minimum vertical motion ($\omega$, $\mu b\,s^{-1}$) during the course of integration for each experiment.

included here since their peak values are mostly located at middle levels. It is apparent that the development of the major mesolow is positively correlated with the explicit precipitation and the upward motion. That is, the lower the central pressure, the more explicit rainfall is produced and the stronger the upward motion. Experiment DES produced the largest total explicit precipitation, followed by exps. NWL, NEV, PES, DHR, CTS and FPS in that order. Detailed results of those simulations are discussed below.

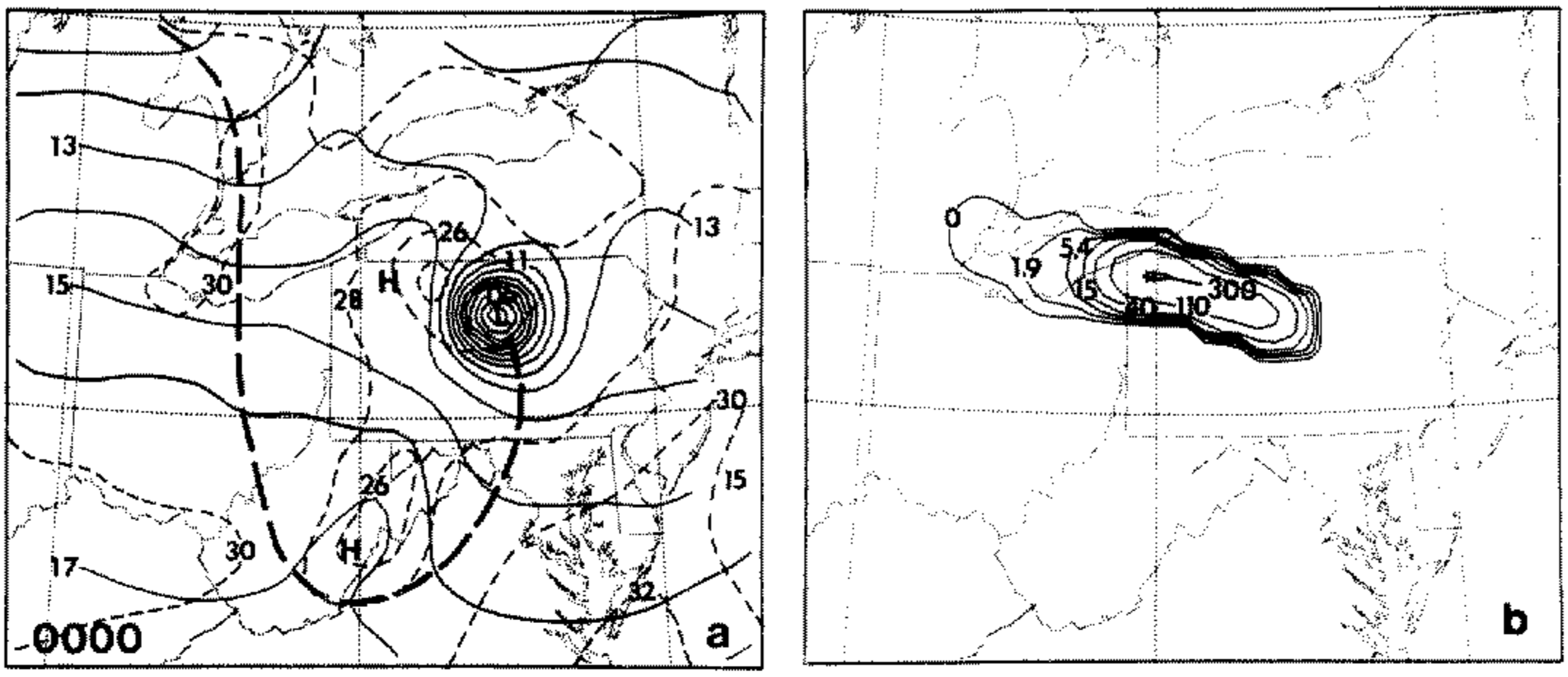


Figure 5. (a) Analyses of sea level pressure (solid lines, mb) and surface temperature (thin dashed lines, °C) from exp. DES (diagnostic explicit simulation) for the time indicated. The heavy dashed lines denote pressure trough. (b) Predicted 12 h accumulated rainfall (mm) for exp. DES.

### (*a*) *Diagnostic explicit simulation*

Without the implicit convective schemes included (exp. DES), the predicted rainfall pattern is very similar to the resolvable-scale counterpart in the semi-implicit control simulation (cf. Figs. 5(b) and 2(e)) and the model fails to produce any precipitation associated with the squall line. Although the simulated path of the mesolow is close to both the observed and the semi-implicit run, the resulting circulation features are unrealistically intense and the mesolow continues its spin-up during the course of integration. At the end of the model integration, the minimum sea level pressure and the point maximum precipitation have respective magnitudes 1004 mb and 315 mm, compared with 1011 mb and 165 mm from the semi-implicit run. The total precipitation exceeded the resolvable-scale portion of the semi-implicit run by almost a factor of two. The point maximum upward motion reaches 500 $\mu b\,s^{-1}$ and its area-averaged value is as strong as 250 $\mu b\,s^{-1}$ (see Table 1 and Fig. 4). As a consequence, an intense mesohigh and a cold dome above it were generated near the tropopause (not shown). The resulting anticyclonic circulation at upper levels almost dominates the entire fine-mesh domain and resembles that produced by a tropical cyclone (see Fig. 9 in Zhang and Fritsch (1987b)). Hoxit *et al.* (1978) and Bosart and Sanders (1981) showed that a similar but much weaker and less extensive structure can be found in observational analyses. This indicates that the pronounced overgeneration of the observed mesolow/meso-vortex is due to the uncontrolled CISK-like instability which resulted from dramatic grid-scale latent heat release. The instantaneous maximum heating rate at the centre of the vortex is found to be about 60 degC $h^{-1}$, compared with 35 degC $h^{-1}$ in exp. CTS (see Fig. 16 in Zhang and Fritsch (1987a)). Koch *et al.* (1985) also showed six separate cases in which excessive cyclogenesis and heating occurred as a result of the absence of a cumulus parametrization scheme in an earlier version of the MASS model.

Due to the poorly controlled instability, the hourly precipitation rate as well as the strength of the mesolow/meso-vortex increases dramatically during the first five model hours when abundant high-$\theta_e$ air is available in the vicinity of the MPWSs, and then decreases with time (see Fig. 3). Similar trends occur with the resolvable-scale circulation. The decreases in the explicit rainfall rate and the weakening of the mesolow/meso-vortex appear to result from the following processes: (1) the moisture supply from a north-

westerly low-level jet could not maintain the moisture consumption by the vortex; this is consistent with a recent theory for tropical cyclone development by Emanuel (1986) and Rotunno and Emanuel (1987); (2) the surrounding compensating subsidence tends to reduce the mid- to upper-level horizontal temperature gradient so that further spin-up is limited; and (3) as the vortex advances south-eastward, it tends to advect additional lower-$\theta_e$ air from the east of the Appalachians which reduces the latent heat release (see Zhang and Fritsch 1986a, 1987a). Moreover, it is important to point out that the highly scale-selective fourth-order horizontal diffusion used in the model ($K_{HO} = 4\times10^4 m^2 s^{-1}$ for the fine mesh) tends to help control the growth rate of the CISK-like instability by suppressing the development of $2\Delta x$-scale waves. Hsie (1983) noted that the smaller-scale details of the evolution of the resolvable-scale convection is sensitive to the magnitude of the diffusion coefficient. It is estimated that there is about a 50% reduction in the amplitude of $2\Delta x$ waves every 6–7 timesteps. However, the strength of the poorly controlled CISK-like instability appears to depend upon the available high-$\theta_e$ air and the model physics incorporated (see Zhang and Fritsch 1987b). In particular, if the present mesolow/meso-vortex developed over an oceanic environment in which the moisture source was from all directions, like the tropical cyclones discussed by Emanuel (1986) and Rotunno and Emanuel (1987), the growth rate could be much larger and growth more persistent.

It is necessary to remark that vertically propagating $2\Delta\sigma$ waves similar to that noted by Kalb (1987) also appeared within the simulated vortex in exp. DES. It is found that this is due to the use of a centre-differencing scheme for vertical advection when the flow propagates through a step-like perturbation which in this case was associated with the surplus of latent heat release over the adiabatic cooling. Meanwhile, the use of a rigid boundary condition (i.e. $\dot{\sigma} = 0$, at $p = p_t$) tends to aggravate the oscillation. However, the $2\Delta\sigma$ oscillation was confined within the radius where the inertial stability reaches a maximum, since large inertial stability tends to inhibit the radial displacement of energy-carrying parcels, whereas the nearly moist adiabatic stratification within the central core of the vortex favours the vertical propagation of the waves (see Smith 1981; Schubert and Hack 1982).

The faster and greater spin-up of the mesolow/meso-vortex in this simulation relative to exp. CTS probably stems from the following two factors: (1) the vertical heating profiles are predominantly located at lower to middle levels (see Fig. 11 in Zhang and Fritsch (1987b)); and (2) the lack of a retarding effect by parametrized deep convection, particularly moist downdraughts. In this regard, it is interesting to note that the 12 h accumulated explicit rainfall pattern and its distribution in exp. DES are similar to the resolvable-scale portion in exps. CTS, but the total rainfall volume in exp. DES is close to the rainfall totals (i.e. parametrized plus grid-resolved) in exp. CTS (see Table 1). This implies that the explicit convection in exp. DES converts a similar amount of moisture into model rainfall as produced by both implicit and explicit convective schemes in exp. CTS. As shown in Zhang and Fritsch (1987b), the explicit convection generally exhibits a heating maximum at a relatively lower level than the parametrized convection. This shifting of the heating maximum to lower levels has been found to be very effective in spinning up a vortex. For example, in a linear analytic study of extratropical cyclogenesis, Gyakum (1983) computed a 24 h central pressure difference of 50 mb when the level of maximum heating was shifted downward by only 200 mb (i.e. from 500 to 700 mb). In numerical studies, Anthes and Keyser (1979) and Anthes *et al.* (1983) found a similar deepening of the mesocyclone when the maximum latent heating occurs at relatively lower levels. It is also evident that the roles of the implicit convective scheme, particularly the parametrized moist downdraughts, are not only to cool the lower

atmosphere and stabilize the vertical column, but also to remove the moisture content that would otherwise be used for explicit condensation and for intensifying the resolvable-scale penetrative circulation (see exp. NPD in Zhang and Fritsch (1987b)). The retarding effect of the implicit convective scheme is so pronounced that the control-simulated area-averaged maximum upward motion is less than half of that in exp. DES. It is important to point out that the implicit convective scheme without parametrized moist downdraughts can also retard the development of the CISK-like instability. For instance, Anthes *et al.* (1983) and Kalb (1987) found significant weakening of mesocyclogenesis when their implicit convective schemes are utilized in combination with the diagnostic explicit formulation (semi-implicit). In addition, Zhang and Fritsch (1987b) showed that the application of the Anthes–Kuo cumulus scheme for both grid meshes to the Johnstown MPWSs (semi-implicit) produced considerable weakening of the mesolow/meso-vortex. The essence of such a retarding effect is clearly due to the fact that *all implicit convective schemes shift the heating maximum to higher levels than explicit condensation would generate*.

Finally, it is important to mention that when the implicit schemes (Fritsch–Chappell and Anthes–Kuo) were used alone, the model successfully reproduced the evolution of the squall line, but totally missed the mesolow/meso-vortex development (see Zhang and Fritsch 1987b). This and the results from exp. DES indicate that the mesolow/meso-vortex is closely linked to the explicit condensation whereas the model squall line is

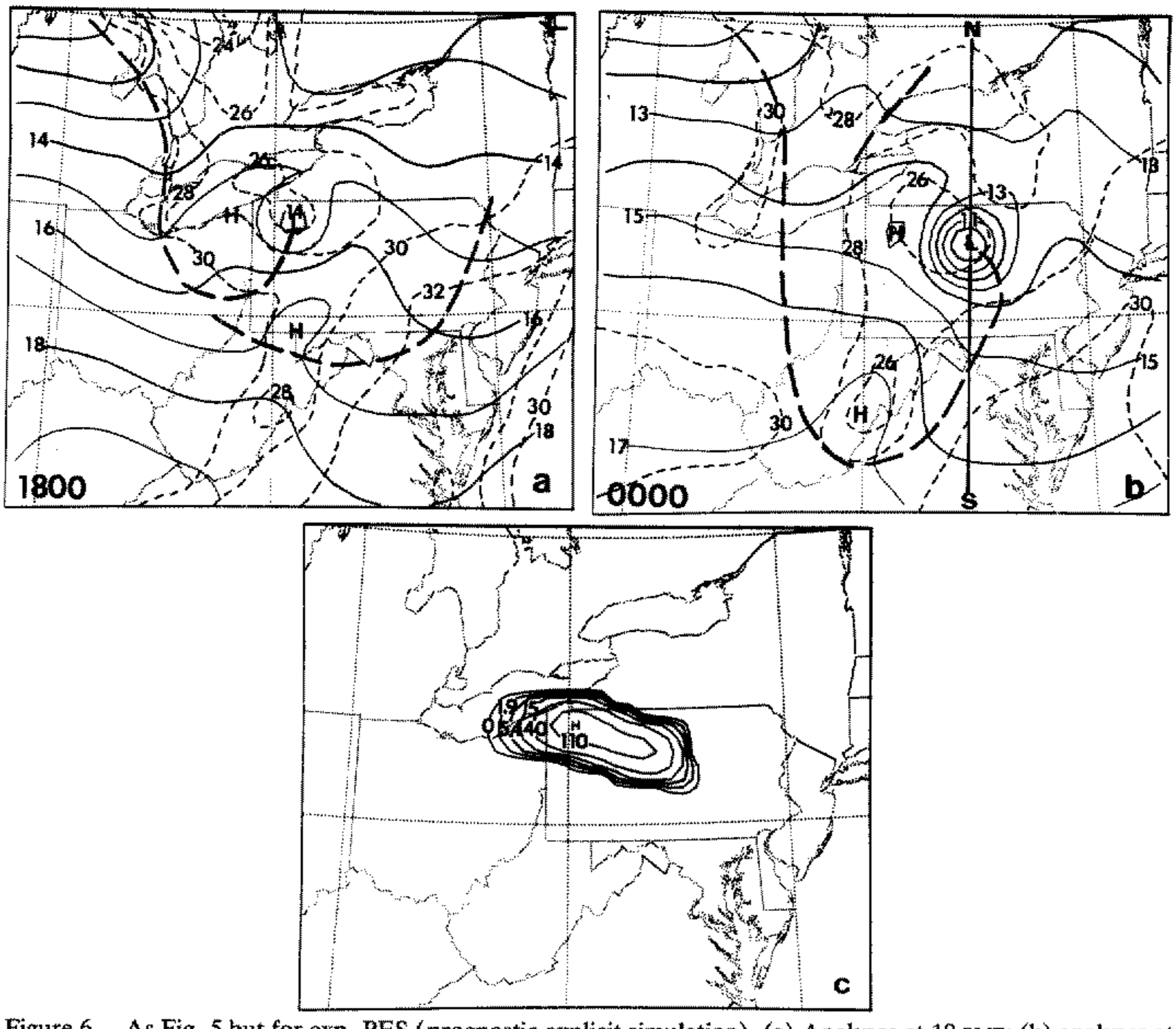


Figure 6. As Fig. 5 but for exp. PES (prognostic explicit simulation). (a) Analyses at 18 GMT; (b) analyses at 00 GMT; (c) predicted 12 h accumulated rainfall (mm).

generated through the parametrized convection. The next few subsections show how these two different rainfall modes are handled by the prognostic explicit representation of moist physics.

### (*b*) *Prognostic explicit simulation*

When the resolvable-scale condensates become fully prognostic (exp. PES), the basic pattern is similar to that produced by the simple supersaturation removal method (see Fig. 6). Specifically, the explicit convective scheme is still unable to reproduce the squall line while the stratiform rainfall associated with the mesolow/meso-vortex is reasonably predicted except that it is excessive. It is noted that because of the initial near-saturated and moist adiabatic conditions over Lake Erie, the centralized upward motion associated with the mid-level short wave started to convert water vapour into cloud water within a couple of timesteps and about 0·75 model hours later, rainwater began to form. Figure 7 shows a vertical cross-section of cloud water content through the mesolow/meso-vortex. Due to the strong upward motion at the centre of the meso-vortex (see Zhang and Fritsch 1987a), the surrounding compensating subsidence tends to dry the air so that the water content is basically confined within the core of the vortex. At upper levels, intense anticyclonic circulation and divergent outflow resulted in the widespread 'cloud anvil'.

Since there is no notable delay in condensation and rainwater conversion, and since both initial conditions and the control simulation indicate a convectively favourable environment over the region traversed by the squall line, it is not likely that the initial conditions of vanishing cloud water and rainwater would affect the reproduction of the squall line. Therefore, a natural question is: Why does the explicit convective scheme fail to reproduce the convective rainfall? Figure 8 shows the 6 h vertical motion ($\omega$, $\mu b\,s^{-1}$) and relative humidity fields at 850 mb. The 850 mb level is chosen because this is roughly the level at which the top of the PBL and lifting condensation level (LCL) are located. Interestingly enough, there is a favourable upward motion band oriented along the region where both the observed and control-simulated squall lines are situated at this time. Correspondingly, a similar shape of higher relative humidity has been created with a maximum value of a little above 90%. It has been found that this banded structure was actually associated with propagating internal gravity waves since the relationship between the vertical motion and surface pressure perturbations is in good agreement

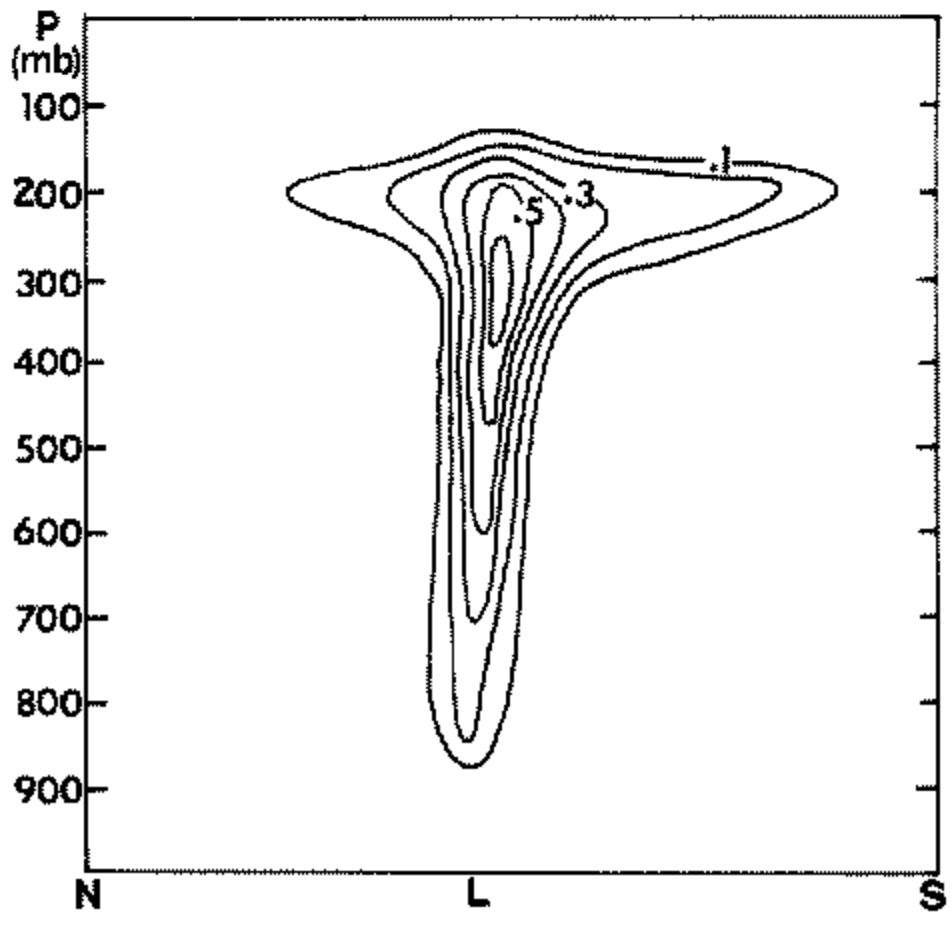


Figure 7. North–south cross-section of 12 h forecast cloud water for exp. PES (see Fig. 6(b) for the location). The contour interval is 0·1 g kg$^{-1}$.

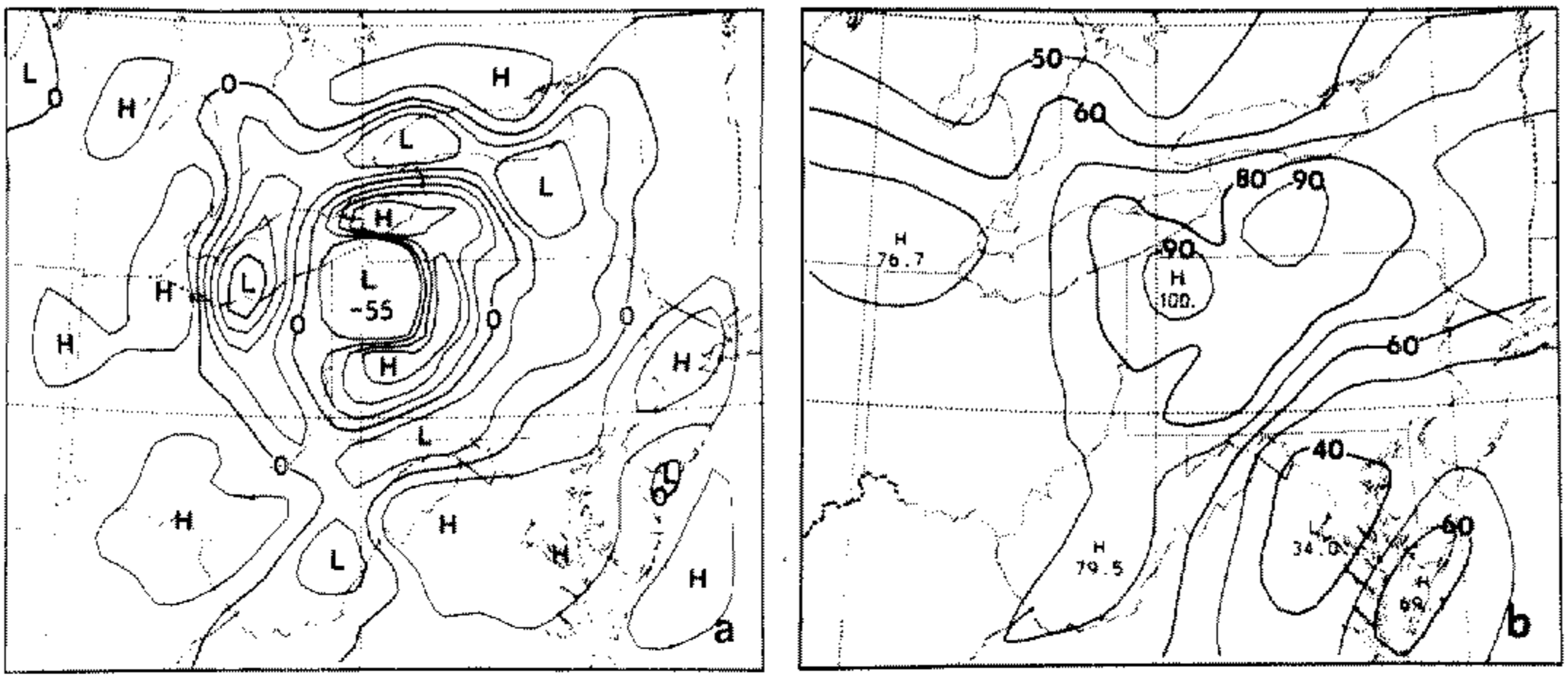


Figure 8. (a) Predicted 6 h vertical motion ($\omega$, $\mu b\,s^{-1}$) at 850 mb verified at 18 GMT. The contour interval is $2\,\mu b\,s^{-1}$. The letters 'H' and 'L' denote the local maximum and minimum values, respectively. (b) As (a) but for relative humidity.

with the gravity wave theory of Gossard and Hooke (1975), Eom (1975) and Uccellini (1975). (The interaction of gravity waves with the squall line is a separate topic and will be discussed in another paper.) The failure of the explicit convective scheme to reproduce the squall line appears to be due to the following factors. In other experiments, the gravity wave was found to propagate eastward significantly faster than the initial near-saturated air mass. After 16 GMT, the wave separated from the original air mass and advanced into a convectively unstable but no longer saturated environment. Since the explicit convective scheme requires a grid-scale saturation to initiate the convection and since, in its absence, other factors such as evaporation and water loading, cannot affect the wave forcing, the banded upward motion in Fig. 8 is much weaker than that in exp. CTS for generating deep convection, particularly in mid to upper levels (not shown). Furthermore, the horizontal grid resolution of 25 km may be too coarse to produce upward motion sufficiently strong to bring the low-level moisture to the LCL. On the other hand, the advantage of an implicit convective scheme (Fritsch–Chappell or Anthes–Kuo, see Zhang and Fritsch (1987b)) is that once the environmental conditions are all favourable, the cumulus scheme sends the parcel instantaneously from the PBL to the upper troposphere to simulate the penetrative convection and no prior saturation is required.

Although an overgeneration of the mesolow/meso-vortex is still apparent in this simulation, the inclusion of condensate time dependence, evaporation and water loading improves the strength of the mesolow/meso-vortex and the associated rainfall as compared with exp. DES. While there is little evidence of resolvable-scale downdraughts due to the evaporation and water loading, and there is little indication of the evaporation-produced cooling from the surface analysis in comparison with exp. CTS, these factors have clearly played an important retarding role in suppressing resolvable-scale circulation and the mesocyclogenesis. To test the importance of the time-dependent effect, one additional experimental simulation was conducted in which the explicit evaporation and instantaneous water loading are incorporated into the diagnostic explicit formulation. The simulated minimum central pressure of the mesolow only improved by 1 mb at the end of 12 h integration (not shown). The significance of the time dependence can also be seen from the rainfall distribution in Fig. 6(c). The transverse dimension of the rainfall pattern is wider, while in the longitudinal direction, there is a delay in the precipitation (but not condensation) at the beginning and light rainfall at a later stage in comparison

with exp. DES. The significance of the water loading and evaporation can be better discussed in the experiments described in the next two subsections.

### (c) *Prognostic explicit simulation without evaporation*

When the evaporation of cloud water and rainwater (exp. NEV) was neglected in exp. PES, no essential changes occurred except that the CISK-like instability became even more unrealistic (see Fig. 9), as expected. Specifically, Table 1 shows that the central pressure of the predicted mesolow is 2 mb deeper and the 12 h accumulated total rainfall volume is about 15% more than in exp. PES. Nevertheless, it is interesting to note in Figs. 3 and 9 that the evaporation of precipitable water had little effect on the hourly rainfall rate during the first five model hours, and the predicted mesolow strength at the sixth model hour is almost the same as in exp. PES. This similarity can be attributed to the nearly saturated and moist adiabatic environment that was initially situated over the Lake Erie area. Thus, little evaporation would be allowed as the liquid water falls through the nearly saturated subcloud layer. However, as the vortex moved southeastward and entered a relatively dry environment, a considerable amount of evaporation occurred (see Fig. 3), retarding the development of the mesolow/meso-vortex. This indicates that the significance of rainfall evaporation depends on the relative humidity in the immediate mesoscale environment.

Even though the evaporation effect is insignificant during first few model hours, the maximum area-averaged vertical motion increased about 12 $\mu b\,s^{-1}$ when the liquid water

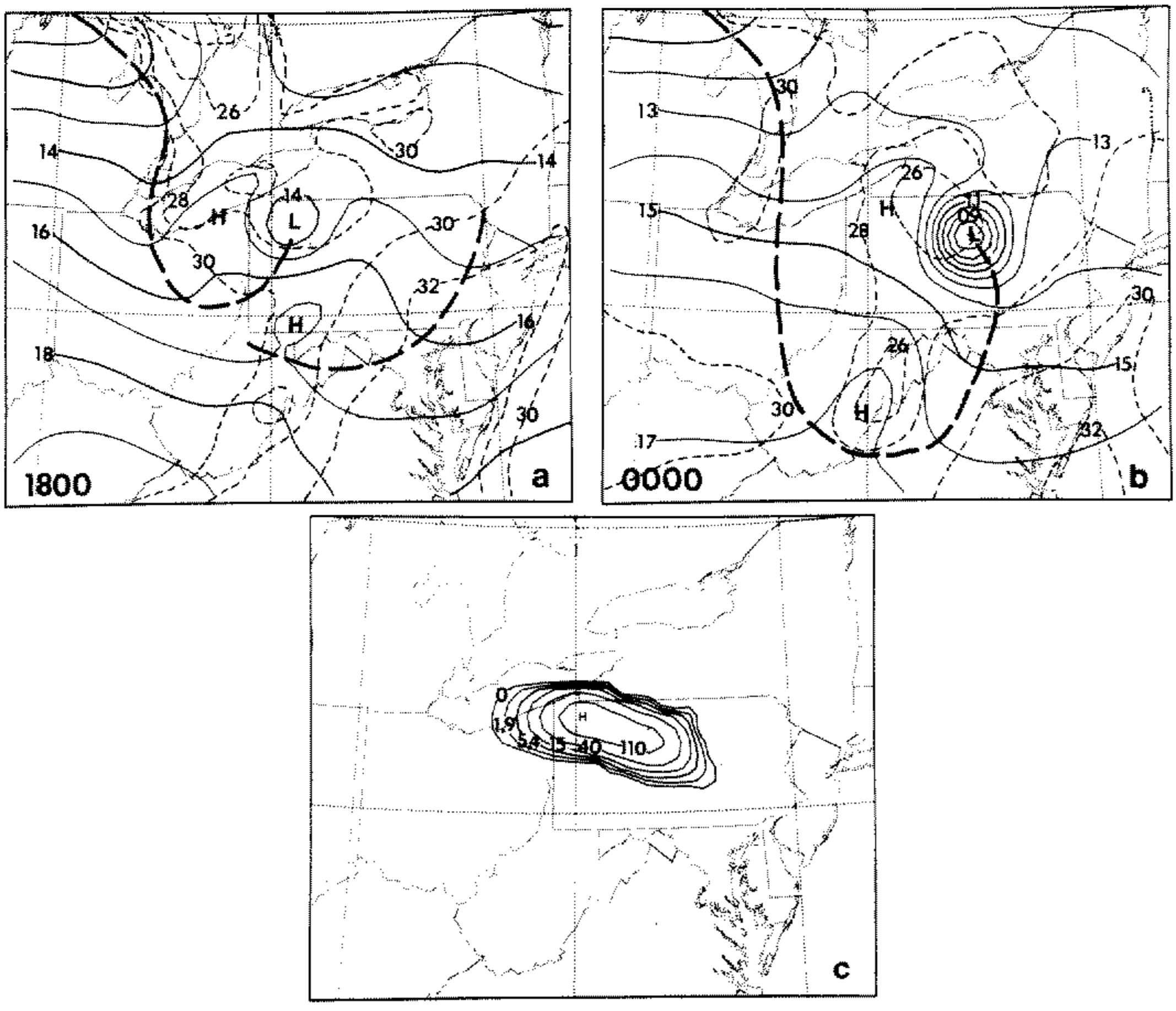


Figure 9. As Fig. 6 but for exp. NEV (no evaporation).

evaporation was excluded. This is comparable to a two-dimensional axisymmetric numerical result by Brown (1979) who found that the rainfall evaporation in his case is capable of driving area-averaged ($2500-10\,000\,km^2$) unsaturated downdraughts with peak strength on the order of $10\,cm\,s^{-1}$. Furthermore, Hsie (1983) found that when the evaporation of liquid water is ignored, the downdraughts associated with a two-dimensional front fail to develop and the accumulated rainfall is significantly greater than when it is included. Note in Figs. 6 and 9 that the incorporation of liquid water evaporation has almost no distinguishable effect on the low-level temperature distribution. Zhang and Fritsch (1987a) showed that the weak surface cool pool associated with the mesovortex was a consequence of the equivalent potential temperature conservation as a parcel ascends within the central core region.

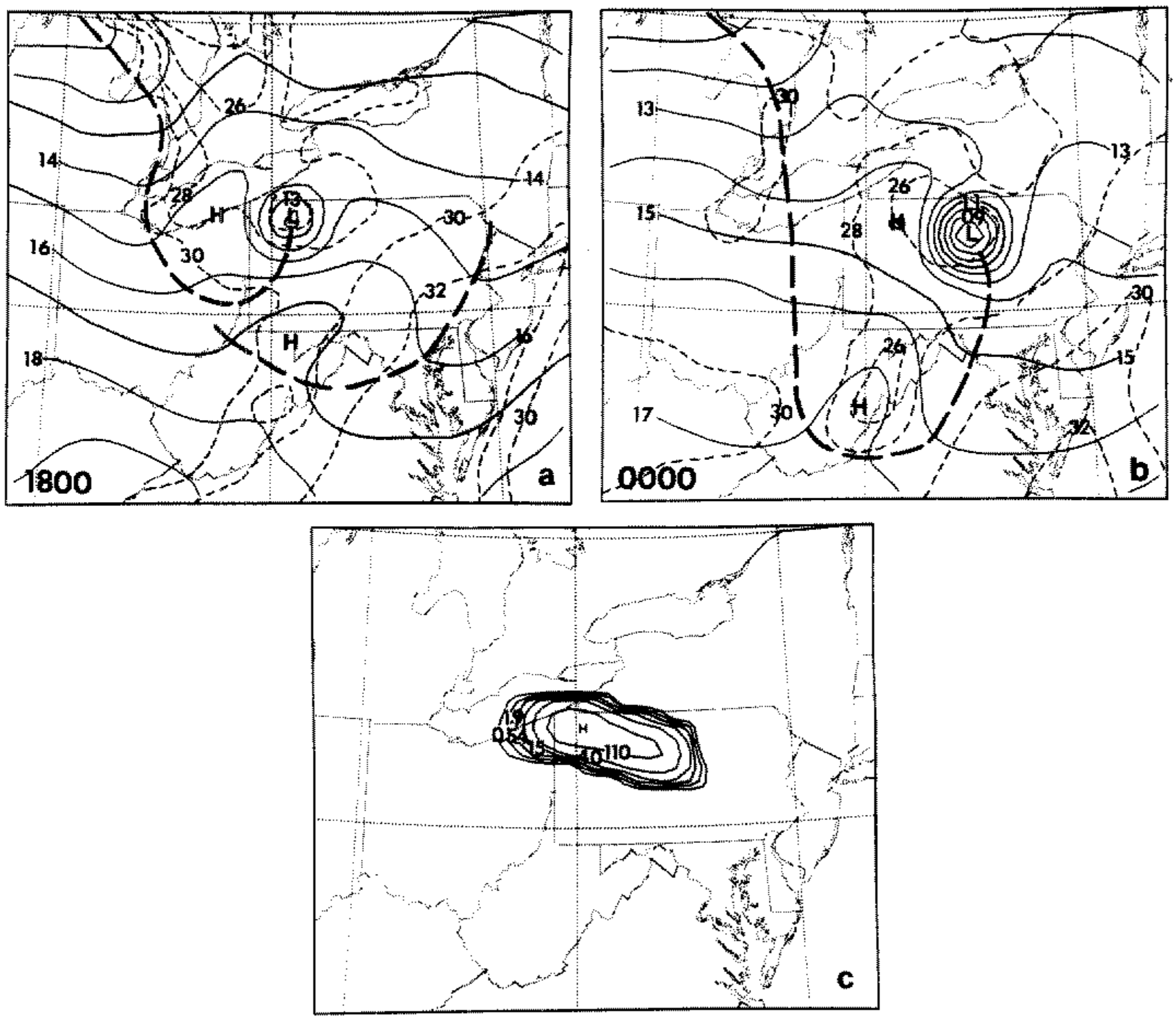


Figure 10. As Fig. 6 but for exp. NWL (no water loading).

### (*d*) *Prognostic explicit simulation without water loading*

When the water loading term from Eq. (12) is ignored (exp. NWL), the mesolow overdeepens substantially as compared with exp. PES (see Fig. 10). The CISK-like instability during the first five hours is only a little alleviated from that in exp. DES, but is worse than in exp. NEV, as shown in Fig. 3. The incorporation of the water loading accounts for a decrease in the area-averaged middle-level vertical motion by $50\,\mu b\,s^{-1}$; and this is about three times more significant than the evaporation effect in suppressing vortex circulation. With both one- and two-dimensional cloud models, Orville *et al.*

(1975) and Orville and Chen (1982) found that the water loading at lower and middle levels of a cloud updraught can lead to a breakdown of the updraught and has very significant influence on cloud development and precipitation evolution. In the present simulation, the upward motion associated with the meso-vortex is so strong and organized that the water loading effect is unable to drive a mesoscale downdraught but can exert only a retardation on the condensation-driven vertical circulation. Nevertheless, compared to reality, the grid-scale vertical motion will not be as strong as the updraughts in a cloud system and the model precipitable water would fall relatively faster through the vertical column. As it is understood, the liquid water tends to form first in association with the maximum vertical motion, and later concentrate at the level above the maximum motion, as shown in Fig. 7. Thus, as the grid spacing increases, the relatively enhanced fall speed of liquid water from mid to upper levels tends to reduce the geopotential height at the levels below, thus causing a retardation of the vertical motion at lower levels, particularly during initial rainwater formation stage. (Note that in this case, the water loading integrated in a vertical column decreases since less water content would remain in the column.) In fact, Molinari and Dudek (1986) utilized a grid resolution of 60 km to simulate the same Johnstown MPWSs as in this study with a similar initial condition, and found that the hydrostatic water loading in one sensitivity experiment prohibited the development of heavy rainfall production. This indicates that the grid-resolution effect on the resolvable divergence/convergence may need to be incorporated into the formulation of raindrop terminal velocity ($v_t$).

Unlike the liquid water evaporation that is effective when encountering an unsaturated condition, the hydrostatic water loading is operative in a saturated environment since only under this condition can liquid water exist. Hence, the water loading effect is more important than the liquid water evaporation in suppressing the vortex circulation in the central core region of the vortex. This appears to be the reason why the predicted mesolow in exp. NWL is much stronger than that in exp. NEV at 6 h when the vicinity of the vortex is close to saturation, and the strength of both mesolows is similar at the end of the simulation since later the meso-vortex gradually entered the unsaturated environment.

### (*e*) *Explicit simulation with double resolution*

Since the explicit simulation with a grid size of 25 km failed to reproduce the convective rainfall associated with the squall line and MCC, the grid length of the model was halved to 12·5 km (exp. DHR) while the domain size, initial data and other conditions are held the same as in exp. PES. As expected, the decrease in horizontal grid spacing allows stronger vertical motion and smaller-scale features to develop, and the model is even more prone to the unrealistic development of CISK-like instability (see Fig. 11). Specifically, the point maximum upward motion ($-\omega$) increased from 324 $\mu b\,s^{-1}$ in exp. PES to 550 $\mu b\,s^{-1}$ in exp. DHR and the strongest mesolow of all the experimental simulations was generated at the sixth model hour. The most discouraging result from this simulation is that the model still fails to reproduce any rainfall associated with the propagating gravity wave that is related to the organized squall line. Thus, it is concluded that the hydrostatic explicit approach is not suitable for the meso-$\beta$-scale simulation of propagating, convectively driven weather systems, since the 12·5 km grid resolution used is close to the lower limit for the validity of the hydrostatic assumption and the initial conditions would be unlikely to affect the model's capability to reproduce the convective mode condensation. The failure of the explicit convective scheme to reproduce the organized convective mode with such a fine resolution appears to be due to the grid-scale vertical motion (upward and downward) not being able to reach the intensity of the

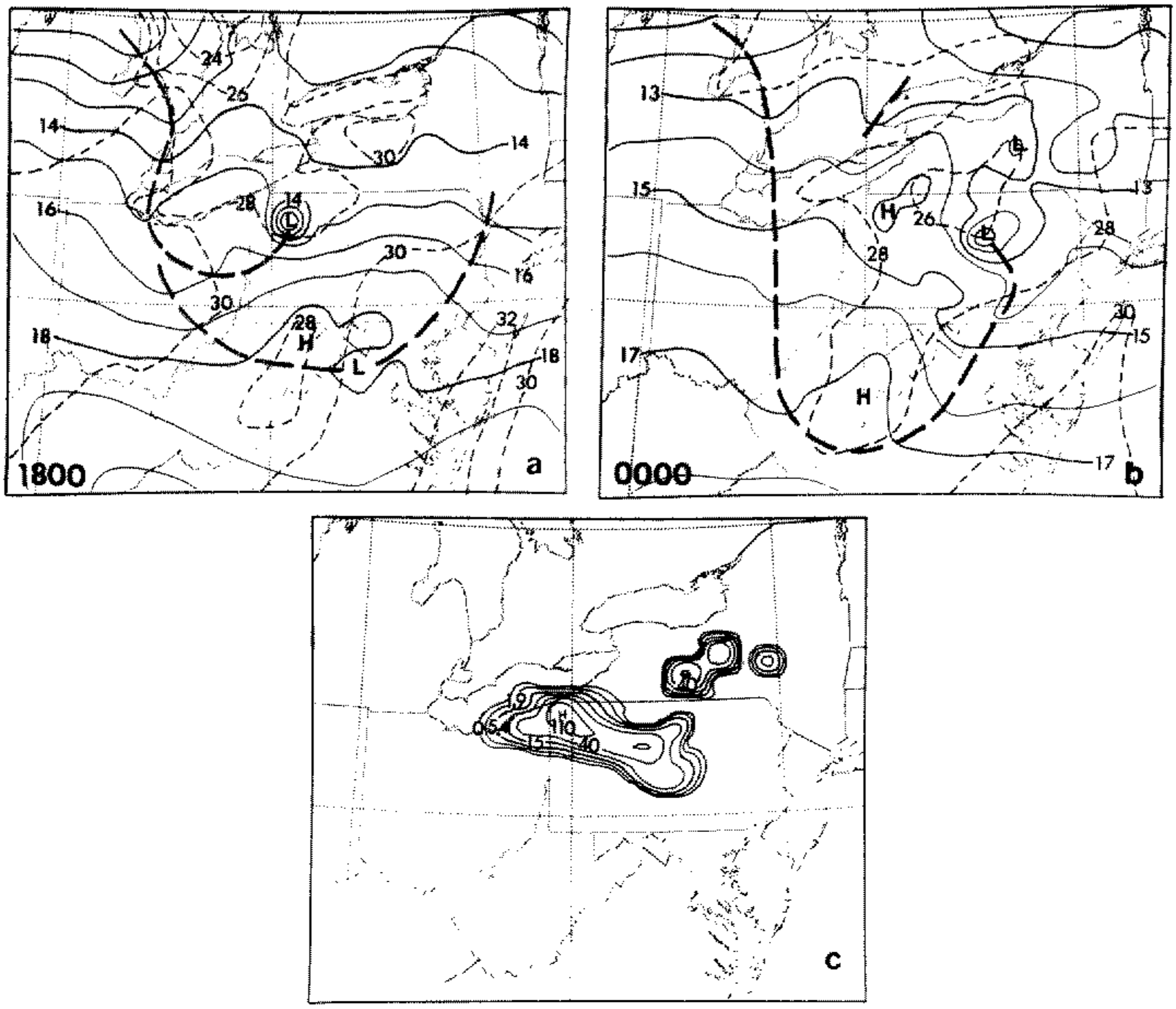


Figure 11. As Fig. 6 but for exp. DHR (double horizontal resolution).

vertical motion typical of a cumulonimbus cloud; the air in the PBL was unable to be lifted sufficiently quickly to the LCL during the passage of the favourable wave forcing. Even if the air parcel could reach the LCL but failed to generate a strong perturbation constructively interacting with the wave, it is apparent that the approaching negative forcing would tend to suppress the convective development (see Fig. 8(a)). It is felt that in order to reproduce the present squall line with the explicit convective scheme, the grid size may need to be further considerably reduced so that individual convective components, such as updraughts, downdraughts and precipitation fallout, can be explicitly resolved. This will require the use of a nonhydrostatic cloud model with a horizontal grid resolution substantially less than 5 km.

There are two areas of concentrated rainfall over central New York that are actually associated with orographic forcing (see Fig. 12 for the terrain distribution). Specifically, as the nearly saturated air mass initially situated over Lake Erie advanced eastward and encountered a favourable upslope motion, a runaway type of the feedback among the latent heat release, moisture convergence and surface pressure fall was triggered. This process appears to occur after the favourable forcing from the gravity wave passed, i.e. by the eighth model hour later as shown in Fig. 3. As a result, a second mesolow developed over this region.

While doubling the horizontal grid resolution increases the magnitude of grid-point vertical motion and its accumulated rainfall volume considerably, their area-averaged values are less than that in exp. PES (see Fig. 3 and Table 1). It appears that as the

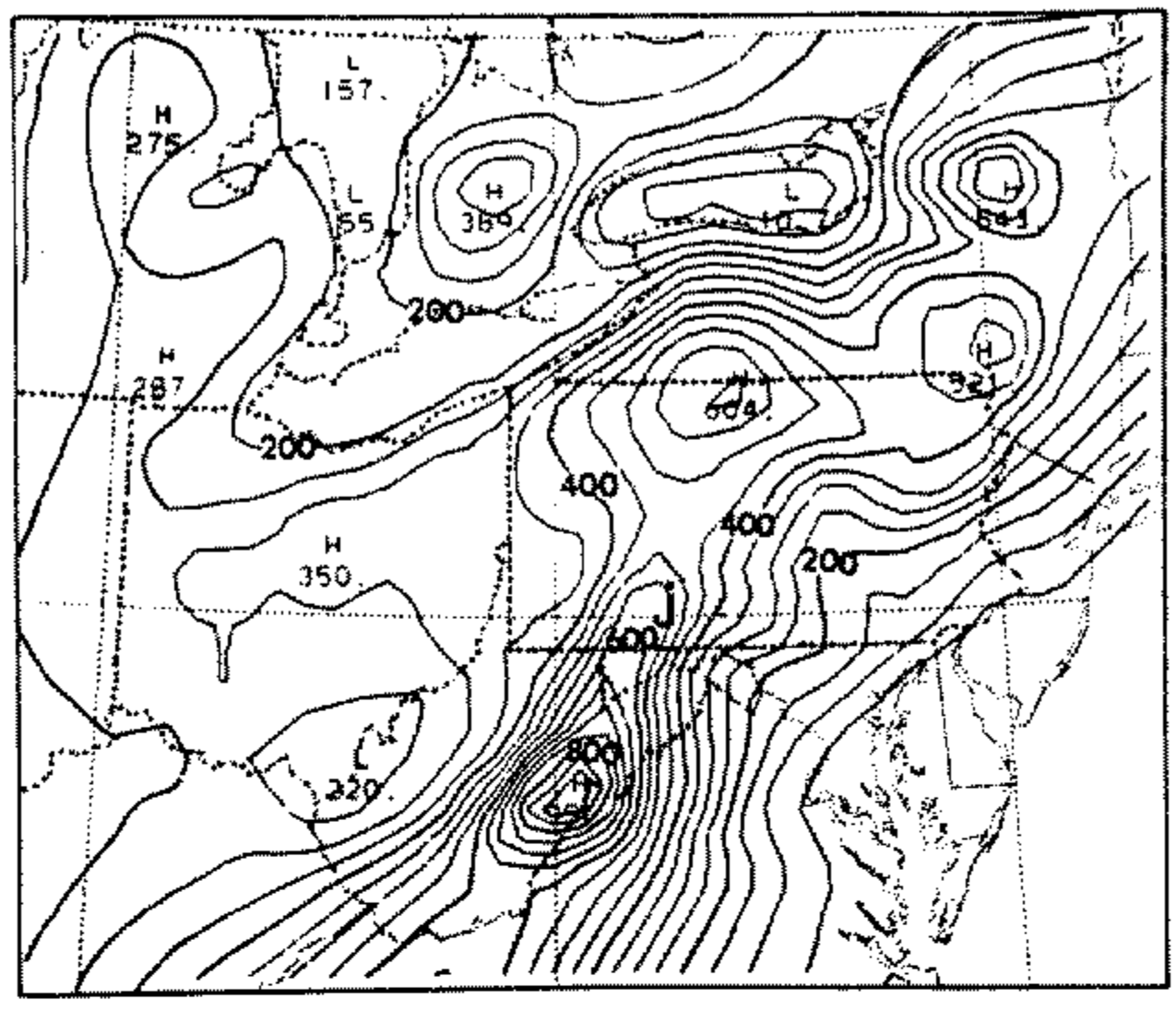


Figure 12. The fine mesh terrain distribution (m) used for this study.

vortex stretches as a result of the above-mentioned positive feedback process, the radius to which the vortex is stiffened becomes smaller (see Smith 1981; Schubert and Hack 1982). Thus, the transverse dimension of heavy rainfall coverage is relatively less extensive, as shown by the 40 and 110 mm contours, in comparison with exp. PES.

### (*f*) *Full physics simulation*

As has been shown, the prognostic explicit scheme was unable to reproduce the convective rainfall on the meso-$\beta$ scale, the behaviour of the CISK-like instability, and the magnitude and distribution of the reproduced stratiform rainfall, were superior to the diagnostic explicit scheme. On the other hand, the implicit convective scheme was responsible for the reproduction of the convective mode but failed to generate the mesolow/meso-vortex, whereas the semi-implicit control simulation sustained the overdevelopment of the meso-vortex. Thus, there is a motivation to investigate the combined effects of the prognostic explicit and implicit convective schemes on the simulation of the Johnstown MPWSs and on the control of the CISK-like instability (exp. FPS).

Figure 13 shows the model-produced surface analyses of convective activity, sea level pressure, the accumulated explicit and total rainfall. Comparisons with the observational analyses of Hoxit *et al.* (1978) (see Fig. 14) and Bosart and Sanders (1981) are very encouraging. First, the simulation successfully reproduced the evolution, size and orientation of the squall line, MCC and embedded mesolow/meso-vortex, as did the control run. The predicted convective activity at 12 h does not conform as well as exp. CTS to the observations. It is, however, regarded as quite satisfactory if a potential bias is considered to be contained in the control simulation. Second, and most strikingly, the CISK-like instability is best handled among all the experimental simulations. Specifically, the pattern and strength of the meso-vortex and mesohigh over western Pennsylvania at 6 h conform exceedingly well to the Hoxit *et al.* analysis (cf. Figs. 13 and 14), i.e. the predicted mesolow is relatively weaker and the mesohigh is stronger than in exp. CTS. Similar evidence holds for the 12 h forecast. Correspondingly, the predicted magnitude of the heaviest rainfall over north-western Pennsylvania is significantly improved. The resulting 12 h accumulated explicit rainfall is about 33% of the precipitation total, compared with 44% in the control simulation. Apparently, those improvements can

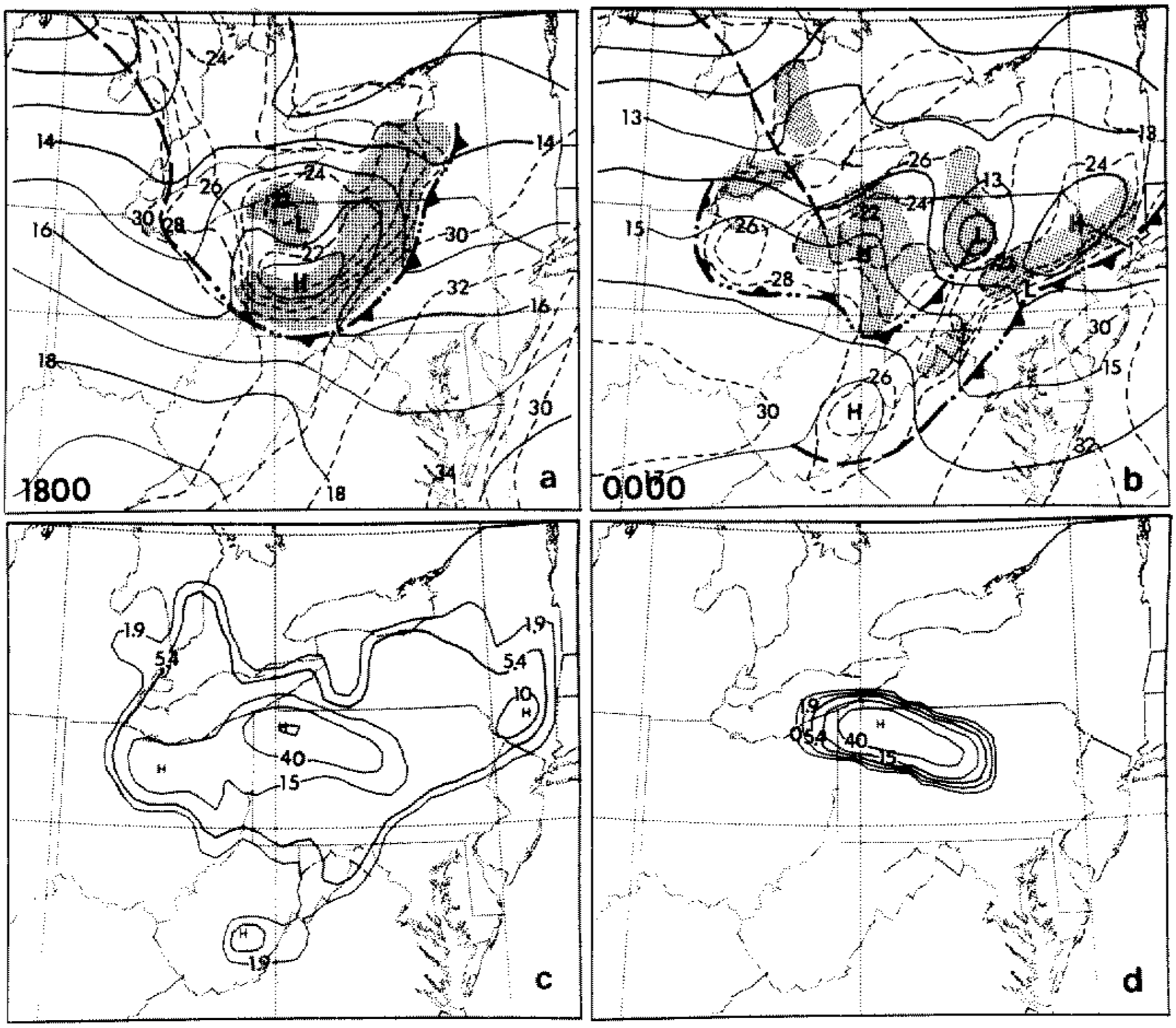


Figure 13. As Fig. 2 (b)–(e) but for exp. FPS (full physics).

largely be attributed to the incorporation of the water loading and liquid water evaporation which help retard the unrealistic development of the CISK-like instability.

It is important to point out that although the strength of the mesolow/meso-vortex improves by about 1 mb and the area-averaged peak upward motion ($-\omega$) reduces by 25 $\mu b\,s^{-1}$ in comparison with exp. CTS, the larger-scale pattern and structure differ only slightly. This indicates that the basic results and conclusions from the control simulation are essentially not affected.

## 5. Discussion

### (a) *Feasibility of an explicit convective scheme for mesoscale modelling*

From the experimental simulations, it appears that an implicit convective scheme is very important for the numerical prediction of convectively driven mesoscale systems even for a grid resolution on the order of 10 km, and that an explicit convective scheme may be suitable only for the stratiform type of rainfall which is forced by mesoscale ascent. The necessity of using an implicit convective scheme even with such a small grid spacing may be due to the fact that within a grid box, say 100 $km^2$, there may be many branches of strong updraughts, downdraughts and compensating subsidence, and some portions may be totally saturated. However, as a whole, the atmosphere within the convective system exhibits conditionally unstable and unsaturated stratification. It is not likely that convective rain would occur in nature in the presence of the mesoscale

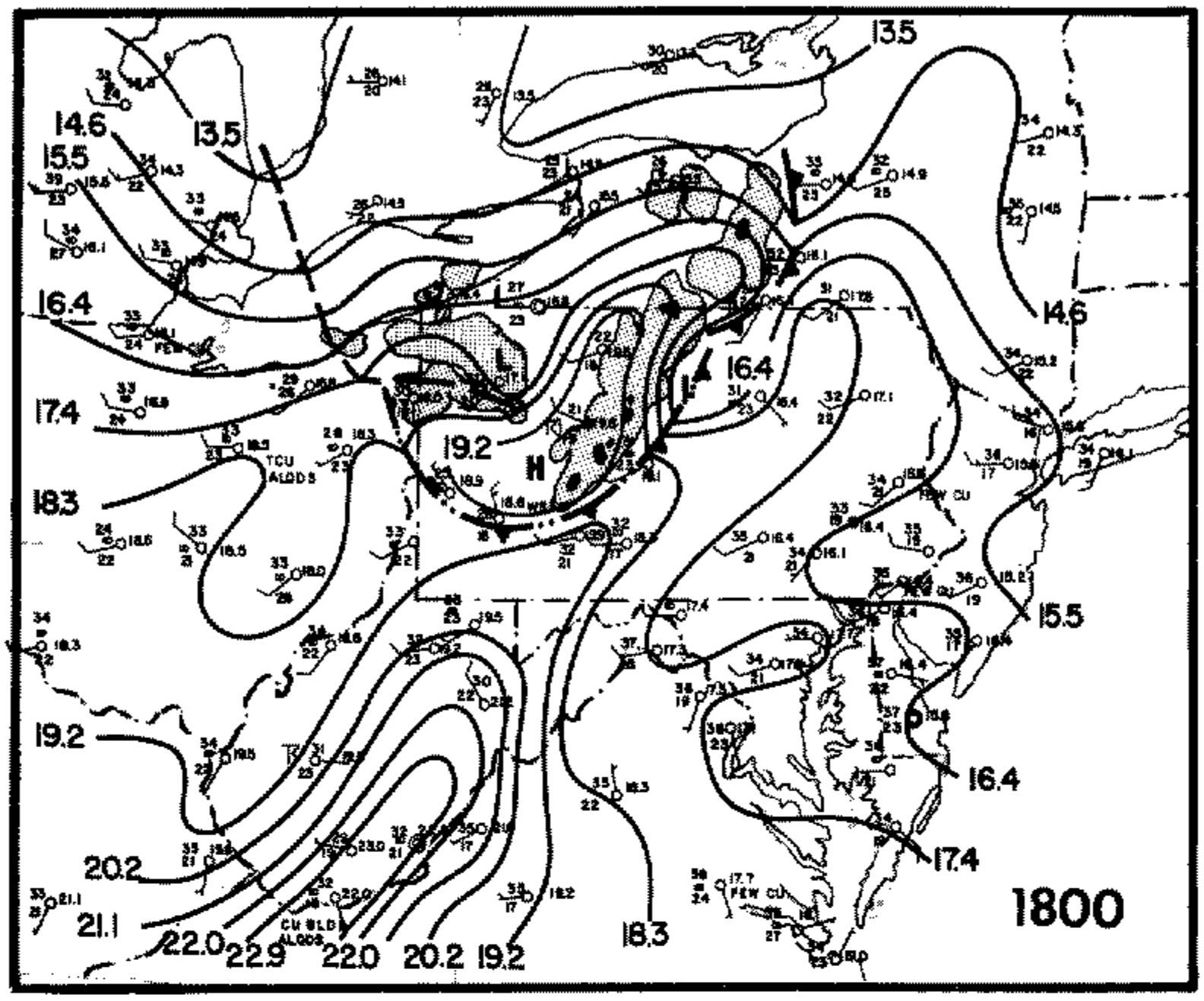


Figure 14. Mesoscale analyses for 18 GMT 19 and 00 GMT 20 July 1977 (adapted from Hoxit *et al.* 1978). Heavy dashed lines indicate troughs. Cold and warm front symbols alternated with double dots indicate moist downdraught outflow boundaries. Light shading denotes level-1 radar echoes and dark shading denotes level-3 radar echoes.

saturation (i.e. over an area with 100 km on a side resolved using a grid size on the order of 10 km). To simulate explicitly such a convective system, apparently the grid size must be small enough for individual convective components to be well resolved. This and other cloud modellers' experiences indicate that the convective downdraughts are very sensitive to the variation of grid resolution, and a grid size at least smaller than 4–5 km is necessary for resolving the downdraught dynamics. Moreover, current available

observed data are generally too coarse to be used for initializing such a fine mesh model because it omits the portion of the atmospheric spectrum between the grid scale and the scale at which the observation takes place. At this stage, even if computer power and initial data could permit such an experiment, it is still questionable whether or not the deep convection can be initiated with the correct temporal and spatial position (predictability). In particular, even in mesoscale nonhydrostatic simulations of squall lines with a horizontal grid size on the order of 1 km, the initiation of the squall line convection is not readily achieved. Due to the characteristically large vertical shear in the squall line environment, it is often difficult to initiate convection from small amplitude heating perturbations (warm bubbles), and thus a density current generated, say, by localized boundary-layer cooling has been invoked (Thorpe *et al.* 1982). Such considerations naturally raise more difficulties for the operational explicit prediction of squall lines and deep convection in general.

Of course, as the grid resolution continues to increase but does not resolve individual convective cells, a different type of difficulty would arise for the implicit approach since there is no clear scale separation between the parametrized and grid-scale convection. It is important to point out that the scale separation concept implied here differs from that proposed by Charney and Eliassen (1964), Ooyama (1971) and Arakawa and Schubert (1974). The original scale separation concept may have been overemphasized during the last two decades since the cumulus parametrization schemes thus developed are only suitable for studying the atmospheric circulation in which convective clouds occur in a slowly varying and quasi-balanced large-scale environment (e.g. tropical depressions, extratropical cyclones), and convection behaves like passive entities. However, many recent observations have revealed a strong interaction between convective and mesoscale draughts, particularly under weak dynamic forcing conditions (Zipser 1977; Houze 1977; Ogura and Chen 1977). In this case, there is no unique relationship between convection and the large-scale circulation, and the evolution of MPWSs tends to be controlled by the thermodynamics and dynamics of convection and the associated mesoscale circulation. To parametrize this type of convection properly, the grid resolution used needs to be large enough to contain several convective elements and yet small enough with respect to the MPWSs being studied.

In contrast, it may be possible for the prognostic explicit scheme to predict correctly MPWSs that are basically forced by larger-scale quasi-stationary forcing, such as temperature contrast between land and water, sloping terrain and those associated with strong baroclinicity and vorticity advection, such as fronts, tropical or marine cyclones (Sanders and Gyakum 1980). It is quite possible, however, that the explicit scheme may encounter a significant delay in the grid-box saturation. Eventually, the model may be able to capture the basic rainfall events. However, there is a strong risk that the resolvable-scale circulation may be overgenerated due to the heating maximum being located at relatively lower levels, and then the model may lose control through the CISK-like processes. Furthermore, in contrast to the Johnstown MPWSs which developed within a weak-gradient large-scale environment so that deep convection basically determined the evolution of the MPWSs, the quasi-stationary forcing and strong baroclinicity would provide the necessary conditions for the development and maintenance of MPWSs. In particular, the large-scale strong deformation tends to transport the convective heating rapidly away from the source region. Although deep convection could modulate the structure and evolution of the larger-scale system, it behaves like a passive entity embedded in and driven by the controlling forcing. Thus, the kind of approach, explicit or implicit, that is used to forecast such MPWSs may not be important as long as the numerical model can predict the large-scale forcing system reasonably well. In fact, a

recent study by Tsou *et al.* (1987) shows that the latent heating plays a much less important role than the vorticity and differential thermal advection in the development of an intense extratropical cyclone.

The present study suggests that the most reliable way to predict the occurrence of different mesoscale precipitating systems in a weakly forced summertime environment correctly is to incorporate simultaneously *both* implicit and prognostic explicit schemes. The advantages of this approach are: (1) both convective schemes play different roles in handling various types and scales of precipitation so that one precipitating mode will not be falsely represented by another; and (2) the model physics corresponds more closely to nature, particularly the necessary retarding effects of parametrized convection, resolvable-scale evaporation and hydrostatic water loading, thus providing a broader scale of interaction between parametrized convection and mesoscale circulation. Even for some predominantly stratiform weather systems (e.g. meso-vortices, Johnston (1981); marine cyclones, Sanders and Gyakum (1980), Emanuel (1986)), the vertical atmospheric column is actually marginally convective (Leary and Rappaport 1987). Incorporation of an implicit convective scheme in combination with a prognostic explicit formulation would assist those precipitating systems to conform to reality. However, there are some disadvantages in including these two schemes simultaneously. For example, this will add more complications into the governing equation system and increase the number of degrees of freedom. Moreover, it will require additional computer time and memory.

### (*b*) *CISK-like instability*

The excessive rainfall 'blow-ups' and dramatic development of the vertical circulation in numerical models are well known and have plagued many modelling investigators for more than two decades. This problem has been recognized as a physical instability entirely related to the resolvable-scale latent heat release (Kasahara 1961). It first arises in a model as a result of vertical destabilization through transport of high-$\theta_e$ air by deformational flow and/or by the daytime mixed-layer development. If mechanisms to release the resulting localized instability are either absent or unsatisfactory and if the vertical column becomes saturated with the lapse rate larger than the moist adiabatic, the shortest resolvable-scale waves tend to grow exponentially with the maximum growth rate permitted by diffusion (Lilly 1960; Kuo 1961), particularly during the initial development stage (see Fig. 9 in Kasahara (1961)). Subsequently, once latent heat release occurs on the resolvable scale, a mesocyclone tends to develop as the wind field rapidly adjusts to the perturbed mass field. A second process of the positive feedback among the latent heat release, larger-scale moisture convergence and surface pressure fall then becomes operative. In particular, because the resolvable-scale heating maximum generally occurs at relatively lower levels, it tends to enhance the lower-level moisture-rich air convergence more efficiently than those with a higher-level heating maximum. The spin-up rate of the vortex depends crucially upon the larger-scale supply rate of high-$\theta_e$ air. Furthermore, as the resulting vorticity exceeds the local Coriolis parameter, inertial stability assists the maintenance of the mesocyclone (Smith 1981; Schubert and Hack 1982; Ooyama 1982) so that within a weak deformational environment, a vortex, once falsely developed, will not readily decay. The present study has clearly shown such a cycle of rapid vortex stretching when abundant high-$\theta_e$ air was available in the vicinity of the Johnstown MPWSs, and of slow decay as the vortex moved into a lower-$\theta_e$ air mass. Although many investigators noted that the model-produced basic sequence was sometimes similar to nature, the model often falsely predicted, if not overproduced, the occurrence of the mesocyclogenesis, and caused frequent model or rainfall 'blow-ups'.

In the past, such a phenomenon has been referred to as gravitational instability

(Kasahara 1961), explicit instability (Molinari and Dudek 1986) and generally as grid-point instability. Actually, they have the same implication, namely, that the resolvable-scale circulation establishes a gravitationally buoyant, unstable column which requires a mechanism of release. These mechanisms involve only a one-scale process. The strong dependence of the model cyclogenesis on the larger-scale supply of high-$\theta_e$ air, as discussed in the previous paragraph, suggests that a 'CISK-like' instability is responsible for the poorly controlled model 'blow-ups'. We use the term CISK-like here instead of CISK because the original formulation assumes the parametrized (rather than the grid-resolved) convection interacting with the larger-scale system to generate a tropical cyclone (Charney and Eliassen 1964; Ooyama 1982). It is apparent that the grid-resolved (i.e. explicit) convection would spin up a tropical-cyclone-type of system even more rapidly than the parametrized convection, but possibly for the wrong reason, as discussed above. To predict different types and different scales of precipitating systems realistically, and to reduce or eliminate the CISK-like instability in the model predictions effectively, numerical modellers may have to incorporate certain model physics as reasonable as in nature, such as evaporation, parametrized deep convection, water loading and melting.

## 6. Concluding remarks

A semi-implicit nested-grid simulation of two different mesoscale precipitating weather systems (a squall line and a MCC) that were responsible for the 19–20 July 1977 Johnstown flood events has been utilized as a control run to investigate the feasibility of an explicit versus implicit approach for meso-$\beta$-scale models, and to examine the roles of the implicit and different explicit model physics in controlling unrealistic development of the CISK-like instability. The explicit convective scheme has been tested with grid sizes of 25 and 12·5 km, respectively. Combined with previous investigators' studies, this research produced the following conclusions:

(1) An implicit convective scheme is very important for predicting convectively driven precipitating systems even with a grid size of the order of 10 km, because the subgrid-scale eddy fluxes should not be neglected on this scale and the convective rainfall in nature does not necessarily occur in the presence of meso-$\beta$-scale saturation.

(2) An explicit convective scheme is capable of generating the stratiform type of rainfall that is associated with mesoscale ascent but is not suitable to be utilized as a unique means of handling different modes of precipitation since (1) the present study indicates the failure of the explicit scheme to reproduce the convective rainfall associated with the squall line and MCC and (2) the explicit scheme tends to produce different degrees of model 'blow-ups', particularly the diagnostic explicit formulation.

(3) Incorporation of appropriate model physics, such as the realistic parametrization of moist convection, resolvable-scale evaporation and hydrostatic water loading, can have significant retarding effects on controlling the CISK-like instability. In particular, parametrized convection tends to reduce the extent of gravitational instability by elevating the maximum heating, and by removing moisture that would otherwise be used for explicit condensation. The water loading has self-control mechanisms when the vertical column becomes falsely saturated in the model, whereas the liquid water evaporation is effective in retarding mesoscale circulation under an unsaturated environment.

(4) Simultaneous incorporation of a prognostic explicit scheme and an implicit convective scheme seems to have the greatest potential success in reproducing various scales and

different types of precipitating weather systems and appears to allow a broader-scale interaction between the parametrized convection and larger-scale environment.

It is, nevertheless, important to point out that some of the conclusions are from one case study only, and the MPWSs being studied here developed within a weak-gradient summertime environment in which the latent heat release and sensible heat redistribution controls the evolution of the MPWSs. Thus, the feasibility of explicit versus implicit approaches for meso-$\beta$-scale models needs to be tested further in other different meteorological situations, particularly with strong dynamic forcing (frontal and/or intense vorticity advection) and quasi-stationary mesoscale forcing, as discussed in section 5. On the other hand, one can have more confidence that if the above conclusions are appropriate for meso-$\beta$-scale models, they will be suitable for the meso-$\alpha$-scale models, except that on the meso-$\alpha$ scales a significant delay of grid-box saturation may become a serious problem.

## Acknowledgments

We are grateful to John Molinari for his critical review. We benefited from helpful discussions with Drs J. M. Brown, J. M. Fritsch, A, Kasahara, R. Rotunno, William Cotton and P. Smolarkiewicz. We thank Mr H. Lansford for his editorial assistance. The first author (DLZ) was supported through the Advanced Study Program and the Mesoscale and Microscale Meteorology Division, National Center for Atmospheric Research (NCAR) which is sponsored by the National Science Foundation. The computations were performed on the NCAR CRAY X-MP.

## References

Anthes, R. A. and Keyser, D. 1979 Tests of a fine-mesh model over Europe and the United States. *Mon. Weather Rev.*, **107,** 963–984

Anthes, R. A. and Warner T. T. 1978 The development of mesoscale models suitable for air pollution and other meteorological studies. *ibid.*, **106,** 1045–1078

Anthes, R. A., Kuo, Y.-H. and Gyakum, J. R. 1983 Numerical simulations of a case of explosive marine cyclogenesis. *ibid.*, **111,** 1174–1188

Arakawa, A. and Schubert, W. H. 1974 Interaction of cumulus cloud ensembles with the large-scale environment, part I, *J. Atmos. Sci.*, **31,** 674–701

Asai, T. 1965 A numerical study of the air-mass transformation over the Japan sea in winter. *J. Meteorol. Soc. Jap.*, **43,** 1–15

Bosart, L. R. and Sanders, F. 1981 The Johnstown flood of July 1977: A long-lived convective storm. *J. Atmos. Sci.*, **38,** 1616–1642

Brown, J. M. 1979 Mesoscale unsaturated downdraft driven by rainfall evaporation: A numerical study. *ibid.*, **36,** 313–338

Chang, C. B., Perkey, D. J. and Kreitzberg, C. W. 1981 A numerical case study of the squall line of 6 May 1975. *ibid.*, **38,** 1601–1615

Charney, J. G. and Eliassen, A. 1964 On the growth of the hurricane depression. *ibid.*, **21,** 68–75

Clark, T. L. 1979 Numerical simulations with a three-dimensional cloud model. Lateral boundary condition experiments and multi-cellular severe storm simulations. *ibid.*, **36,** 2191–2215

Cotton, W. R. and Tripoli, G. J. 1978 Cumulus convection in shear flow—Three-dimensional numerical experiments. *ibid.*, **35,** 1503–1521

Emanuel, K. A. 1986 An air–sea interaction theory for tropical cyclones. Part I: Steady state maintenance. *ibid.*, **43,** 585–604

Eom, J. 1975 Analysis of the internal gravity wave occurrence of April 19, 1970 in the Midwest. *Mon. Weather Rev.*, **103,** 217–226

Frank, W. M. 1983 The cumulus parameterization problem. *ibid.*, **111,** 1859–1871

Frank, W. M. and Cohen, C. 1985 Properties of tropical cloud ensembles estimated using a cloud model and an observed updraft population. *J. Atmos. Sci.*, **42,** 1911–1928

Fritsch, J. M. and Chappell, C. F. 1980 Numerical prediction of convectively driven mesoscale pressure systems. Part I: Convective parameterization. *ibid.*, **37,** 1722–1733

Gossard, E. E. and Hooke, W. H. 1975 'Waves in the atmosphere'. In *Developments in atmospheric science*. Vol. 2. Elsevier Scientific

Gyakum, J. R. 1983 On the evolution of the QE II storm. II: Dynamic and thermodynamic structure. *Mon. Weather Rev.*, **111,** 1156–1173

Haltiner, G. J. and Williams, R. T. 1980 *Numerical prediction and dynamic meteorology*. John Wiley & Sons

Houze, R. A., Jr. 1977 Structure and dynamics of a tropical squall-line system. *Mon. Weather Rev.*, **105,** 1540–1567

Hoxit, L. R., Maddox, R. A., Chappell, C. F., Zuckerberg, F. L., Mogil, H. M., Jones, I., Greene, D. R., Saffle, R. E. and Scofield, R. A. 1978 'Meteorological analysis of the Johnstown, Pennsylvania, flash flood, 19–20 July 1977'. NOAA Tech. Rep. ERL 401-APCL43

Hsie, E.-Y. 1983 'Frontogenesis in a moist atmosphere'. Ph.D. thesis, Department of Meteorology, The Pennsylvania State University

Hsie, E.-Y., Anthes, R. A. and Keyser, D. 1984 Numerical simulation of frontogenesis in a moist atmosphere. *J. Atmos. Sci.*, **41,** 2581–2594

Johnston, E. C. 1981 'Mesoscale vorticity centers induced by mesoscale convective complexes'. M.S. thesis, University of Wisconsin. Department of Meteorology

Kalb, M. W. 1987 The role of convective parameterization in the simulation of a Gulf coast precipitation system. *Mon. Weather Rev.*, **115,** 214–234

Kasahara, A. 1961 A numerical experiment on the development of a tropical cyclone. *J. Meteorol.*, **18,** 259–282

Kessler, E. 1969 On the distribution and continuity of water substance in atmospheric circulation. *Meteorol. Monogr.*, **27.** American Meteorological Society

Klemp, J. B. and Wilhelmson, R. B. 1978 The simulation of three-dimensional convective storm dynamics. *J. Atmos. Sci.*, **35,** 1070–1096

Koch, S. E., Skillman, W. C., Kocin, P. J., Wetzel, P. J., Brill, K. F., Keyser, D. A. and McCumber, M. C. 1985 Synoptic scale forecast skill and systematic errors in the MASS 2.0 model. *Mon. Weather Rev.*, **113,** 1714–1737

Koss, W. J. 1976 Linear stability analysis of CISK-induced disturbances: Fourier component eigenvalue analysis. *J. Atmos. Sci.*, **33,** 1195–1222

Kuo, H. L. 1961 Convection in conditionally unstable atmospheres. *Tellus*, **13,** 441–459

Leary, C. A. and Houze, R. A., Jr. 1979 Melting and evaporation of hydrometeors in precipitation from the anvil clouds of deep tropical convection. *J. Atmos. Sci.*, **36,** 669–679

Leary, C. A. and Rappaport, E. N. 1987 The life cycle and internal structure of a mesoscale convective complex. *Mon. Weather Rev.*, **115,** 1503–1527

Lilly, D. K. 1960 On the theory of disturbances in a conditionally unstable atmosphere. *ibid.*, **88,** 1–17

Liu, J. Y. and Orville, H. D. 1969 Numerical modeling of precipitation and cloud shadow effects on mountain-induced cumuli. *J. Atmos. Sci.*, **26,** 1061–1074

Lord, S. J., Willoughby, H. E. and Piotrowicz, J. M. 1984 Role of a parameterized ice-phase microphysics in an axisymmetric, nonhydrostatic tropical cyclone model. *ibid.*, **41,** 2836–2848

Maddox, R. A. 1983 Large-scale meteorological conditions associated with midlatitude, mesoscale convective complexes. *Mon. Weather Rev.*, **111,** 1475–1493

Martin, C. L. and Pielke, R. A. 1983 The adequacy of the hydrostatic assumption in sea breeze modeling over flat terrain. *J. Atmos. Sci.*, **40,** 1472–1481

Molinari, J. and Dudek, M. 1986 Implicit versus explicit convective heating in numerical weather prediction models. *Mon. Weather Rev.* **114,** 1822–1831

Moncrieff, M. W. and Miller, M. J. 1976 The dynamics and simulation of tropical cumulonimbus and squall lines. *Q. J. R. Meteorol. Soc.*, **102,** 373–394

Nickerson, E. C., Richard, E. R., Rosset, R. and Smith, D. R. 1986 The numerical simulation of clouds, rain, and airflow over the Vosges and Black Forest Mountains: A meso-$\beta$ model with parameterized microphysics. *Mon. Weather Rev.*, **114,** 398–414

Ogura, Y. and Chen, Y. L. 1977 A life history of an intense mesoscale convective storm in Oklahoma, *J. Atmos. Sci.*, **33,** 1458–1476

Ooyama, K. V. 1971 A theory on parameterization of cumulus convection. *J. Meteorol. Soc. Jap.*, **49,** special issue, 744–756

1982 Conceptual evolution of the theory and modeling of the tropical cyclone. *ibid.*, **60,** 369–379

Orlanski, I. 1975 A rational subdivision of scales for atmospheric processes. *Bull. Am. Meteorol. Soc.*, **56,** 527–530

1981 The quasi-hydrostatic approximation. *J. Atmos. Sci.*, **38,** 572–582

Orville, H. D. and Chen, J.-M. 1982 Effect of cloud seeding, latent heat of fusion, and condensate loading on cloud dynamics and precipitation evolution: A numerical study. *ibid.*, **39,** 2807–2827

Orville, H. D. and Kopp, F. J. 1977 Numerical simulation of the life history of a hailstorm. *ibid.*, **34,** 1596–1618

Orville, H. D. and Myers, C. G. 1975 The dynamics and thermodynamics of precipitation loading. *Pure Appl. Geophys.*, **113,** 983–1004

Perkey, D.J. and Kreitzberg, C. W. 1976 A time-dependent lateral boundary scheme for limited-area primitive equation models. *Mon. Weather Rev.*, **104,** 744–755

Perkey, D. J. and Maddox, R. A. 1985 A numerical investigation of a mesoscale convective system. *ibid.*, **113,** 553–566

Phillips, N. A. 1978 'The nested grid model'. NOAA Tech. Rep. NWS. Available from ESIC (D822), NOAA, 6009 Executive Boulevard, MD 20852

Pointin, Y. 1985 Numerical simulation of organized convection. Part I: Model description and preliminary comparisons with squall line observations. *J. Atmos. Sci.*, **42,** 155–172

Rockwood, A. A., Bartels, D. L. and Maddox, R. A. 1984 'Precipitation characteristics of a dual mesoscale convective complex'. NOAA Tech. Rep., ERL/ESG-6

Rosenthal, S. L. 1978 Numerical simulation of tropical cyclone development with latent heat release by the resolvable scales. I: Model description and preliminary results. *J. Atmos. Sci.*, **35,** 258–271

1979 The sensitivity of simulated hurricane development to cumulus parameterization details. *Mon. Weather Rev.*, **107,** 193–197

Ross, B. B. and Orlanski, I. 1982 The evolution of an observed cold front. Part I: Numerical simulation. *J. Atmos. Sci.*, **39,** 296–327

Rotunno, R. and Emanuel, K. A. 1987 An air–sea interaction theory for tropical cyclones. Part II: Evolutionary study using a nonhydrostatic axisymmetric numerical model. *ibid.*, **44,** 542–561

Sanders, F. and Gyakum, J. R. 1980 Synoptic-dynamic climatology of the "bomb". *Mon. Weather Rev.*, **108,** 1589–1606

Schubert, W. H. and Hack, J. J. 1982 Inertial stability and tropical cyclone development. *J. Atmos. Sci.*, **39,** 1687–1697

Smith, R. K. 1981 The cyclostrophic adjustment of vortices with application to tropical cyclone modification. *ibid.*, **38,** 2021–2030

Thorpe, A. J., Miller, M. J. and Moncrieff, M. W. 1982 Two-dimensional convection in non-constant shear: A model of mid-latitude squall lines. *Q. J. R. Meteorol. Soc.*, **108,** 739–762

Tracton, M. S. 1973 The role of cumulus convection in the development of extra-tropical cyclones. *Mon. Weather Rev.*, **101,** 573–593

Tsou, C.-H., Smith, P. J. and Pauley, P. M. 1987 A comparison of adiabatic and diabatic forcing in an intense extratropical cyclone system. *ibid.*, **115,** 763–786

Uccellini, L. W. 1975 A case study of apparent gravity wave initiation of severe convective storms. *ibid.*, **103,** 497–513

Yamasaki, M. 1977 A preliminary experiment of the tropical cyclone without parameterizing the effects of cumulus convection. *J. Meteorol. Soc. Jap.*, **55,** 11–30

Zhang, D.-L. and Anthes, R. A. 1982 A high-resolution model of the planetary boundary layer—sensitivity tests and comparisons with SESAME-79 data. *J. Appl. Meteorol.*, **21,** 1594–1609

Zhang, D.-L. and Fritsch, J. M. 1986a Numerical simulation of the meso-$\beta$ scale structure and evolution of the 1977 Johnstown flood. Part I: Model description and verification. *J. Atmos. Sci.*, **43,** 1913–1943

1986b A case study of the sensitivity of the numerical simulation of mesoscale convective systems to varying initial conditions. *Mon. Weather Rev.*, **114,** 2418–2431

1987a Numerical simulation of the meso-$\beta$ scale structure and evolution of the 1977 Johnstown flood. Part II: Inertially stable warm-core vortex and the mesoscale convective complex. *J. Atmos. Sci.* **44,** 2593–2612

1987b Numerical sensitivity experiments of varying model physics on the structure, evolution and dynamics of two mesoscale convective systems. *ibid.* (to appear)

Zhang, D.-L., Chang, H.-R, Seaman, N. L., Warner, T. T. and Fritsch, J. M. 1986 A two-way interactive nesting procedure with variable terrain resolution. *Mon. Weather Rev.*, **114,** 1330–1339

Zipser, E. J. 1977 Mesoscale and convective-scale downdrafts as distinct components of squall-line circulation. *ibid.*, **105,** 1568–1589